The potential distribution in the quantized Hall effect

Document Version:
Publisher's PDF, also known as Version of Record (includes final page, issue and volume numbers)

Please check the document version of this publication:

• A submitted manuscript is the version of the article upon submission and before peer-review. There can be important differences between the submitted version and the official published version of record. People interested in the research are advised to contact the author for the final version of the publication, or visit the DOI to the publisher's website.
• The final author version and the galley proof are versions of the publication after peer review.
• The final published version features the final layout of the paper including the volume, issue and page numbers.

Link to publication

THE POTENTIAL DISTRIBUTION
IN THE QUANTIZED HALL EFFECT

P.F. FONTEIN

THE POTENTIAL DISTRIBUTION
IN THE QUANTIZED HALL EFFECT

PROEFSCHRIFT

Ter verkrijging van de graad van doctor aan de Technische
Universiteit Eindhoven, op gezag van de Rector Magnificus,
prof. ir. M. Tels, voor een commissie aangewezen door het
College van Dekanen in het openbaar te verdedigen op
vrijdag 5 oktober 1990 te 14.00 uur

door

PETRUS FRANCISCUS FONTEIN

geboren te Geldrop

Dit proefschrift is goedgekeurd door de promotor:

Prof. Dr. J.H. Wolter

en de copromotor:

Dr. ir. F.A.P. Blom

CONTENTS

Contents

CHAPTER 1

ABOUT THE SUBJECT MATTER OF THIS THESIS

Ever since the discovery of the quantized Hall effect[1,2] in 1980, localization of electrons in high magnetic fields is considered to be essential to create Hall plateaus. Several approaches exist to incorporate this localization concept into a physical microscopic model. Since these approaches predict different current distributions, a detailed knowledge of the current distribution is one of the means to increase our insight in the localization problem and thus our understanding of the quantized Hall effect. It is the aim of this thesis to investigate which of these theoretical approaches matches the experimental situation. This investigation includes numerical calculations and predominantly experimental observations.

The results of a quantized Hall measurement are presented in Fig. 1.1. A current is sent through a Hall bar structure, which contains a so-called two-dimensional electron gas. The Hall voltage and the Shubnikov-de Haas voltage are measured as a function of the magnetic field strength. These are the voltage drops across and along the direction of the current, respectively. The Hall resistance and the Shubnikov-de Haas resistance are obtained from the division of these voltages by the current. It is evident from Fig. 1.1 that the Hall resistance shows perfectly quantized plateaus and that these plateaus are accompanied by deep minima of almost zero resistance in the Shubnikov-de Haas oscillations.

Explanations of these phenomena up to now all invoke the concept of localization. Localized electrons have a wave function with a limited spatial extent; their motion is restricted to a finite area. These states occur easily in the presence of a magnetic field, since in the absence of scattering the classical cyclotron orbits of the electrons drift along equipotential lines. Thus a closed equipotential loop in the two-dimensional electron gas may localize electrons. In fact, the entire area surrounded by such a loop may be localized. Since these equipotential loops are caused by nearly every kind of inhomogeneity in the electrostatic potential, localization will certainly be present.

How does this localization enter the problem of the quantized Hall effect? As long as the Fermi energy lies in the region of the localized states and the temperature is sufficiently low, the Shubnikov-de Haas resistance is nearly zero due to the absence of scattering of the mobile electrons. Also the addition of some electrons to the localized states does not change the conductive properties of the non-localized states, and hence the Hall resistance remains constant. However, these hand-waving arguments are not yet a satisfactory model of the quantized Hall effect. Such a model should explain many details like the temperature dependence or the width of the Hall plateaus and Shubnikov-de Haas minima. The key to a better understanding of the quantized Hall effect is probably the comprehension of the localization of electrons in two-dimensional electron systems subjected to a strong magnetic field. One way to attack this problem is to study which parts of the

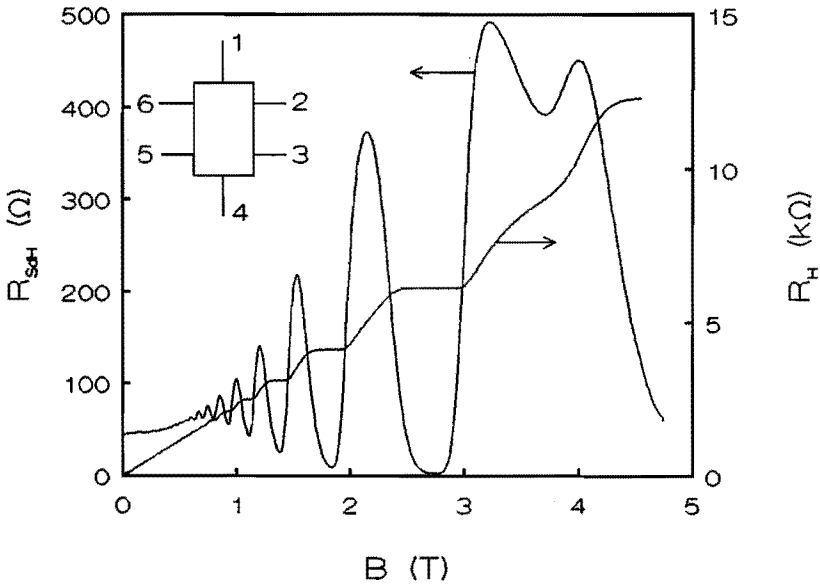**Fig. 1.1** *Typical experimental recordings of the Hall resistance R_H (= V_{26}/I_{14}) and the Shubnikov-de Haas resistance R_{SdH} (= V_{23}/I_{14}), as a function of the magnetic field B. Clearly visible are the plateaus in R_H, which appear at the same values of the magnetic field as the minima in R_{SdH}. The measurement was performed on a $GaAs/Al_xGa_{1-x}As$ heterostructure at a temperature of 1.5 K.*

sample are localized and which parts are contributing to the current. In other words: "How is the current distributed?".

From a theoretical point of view several possibilities exist. The first, and simplest, case would be a homogeneous current distribution with a constant Hall field and thus a linearly increasing Hall potential as a function of position in a direction perpendicular to the current. In this case the density of states is thought to be independent of position. Second, it could be that narrow current paths are percolating through regions of localized states. Because under quantized Hall conditions the electrons move along equipotential lines these percolating paths can be regarded as lines of constant height like in an Alpine landscape, with the hills and valleys containing localized states. As a third possibility one could argue that in a realistic sample the presence of the confining potential at the edges causes extended states to occur along the boundary of the sample. It is thus possible that edge effects cannot be neglected and are of major importance for the observation of the quantized Hall effect.

These three classes of current distributions each have their own supporting models[3-9]. A discussion of these models is given in chapter 3, after the discussion of the two-dimensional electron gas in chapter 2. These selected models are representative for the field of research and the topics discussed in this thesis.

The main topic of this thesis consists of chapters 4, 5 and 6, where we present our results of the investigations on the current distribution. We have organized the results as described in the following paragraphs.

Since we tried earlier to convey the idea that inhomogeneities are important to obtain localization and hence to obtain the quantized Hall effect, we discuss in chapter 4 the presence and magnitude of inhomogeneities. In addition, we present the results of numerical calculations performed on inhomogeneous two-dimensional electron systems in a magnetic field. These calculations are meant to get a clearer picture of the sometimes surprising influences of sample inhomogeneities on the current distribution and hence on the experimental results.

Of course, a direct measurement is the best determination of the occurrence and the position of extended states. This is the topic of chapter 5. Several investigations have been carried out on this subject by other workers in this field[10,11]. All of them apply electrical contacts to the interior of the two-dimensional electron gas. In those experiments the magnitude of the Hall voltage developed

across two internal contacts is used to determine the magnitude of the current flow in between those two contacts. Their results seem to indicate that in between the plateaus the current is more or less homogeneously distributed. But inside a plateau region the current and potential distribution appear to be highly inhomogeneous and strongly dependent on the magnitude of the magnetic field, see Fig. 1.2. In these measurements, however, the electrical contacts influence the current distribution and in this respect the influence of the electrical contacts is questionable. Preferably such a measurement should be performed without using electrical contacts. In chapter 5 we present results of a contactless potential measurement. This measurement is based on a technique which makes use of the linear electro-optic effect. It turns out that the current distribution we observe with this technique completely differs from the one discussed above.
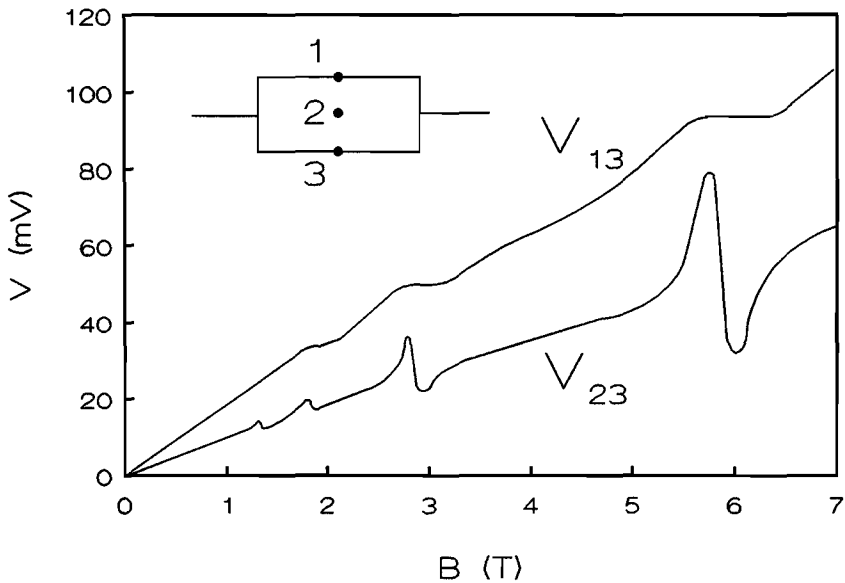
Fig. 1.2 *Experimental results of Ebert et al.[10] obtained on a Hall bar structure with internal electrical contacts. In between the plateaus the drop of the Hall potential is more or less evenly distributed over the different contacts, indicating an almost homogeneous current distribution. However, it is evident that inside the plateau region the potential distribution and hence the current distribution, as deduced from Fig. 1.2, are far from homogeneous.*

Finally, in chapter 6 we address the question of the necessity of sample edges for the quantized Hall effect to occur. We present unique measurements of the quantized Hall effect on samples with a Corbino geometry, which insures that edges do not connect the current contacts. In principle, these measurements show a striking resemblance to a thought experiment by Laughlin[8,9]. Laughlin's model of the quantized Hall effect, which we discuss in chapter 3, is based on this thought experiment. Our measurements on the Corbino structures reveal that under realistic experimental conditions the quantized Hall effect is probably restricted to Hall bar structures, for reasons we show in chapter 6.

CHAPTER 2

PROPERTIES OF THE TWO-DIMENSIONAL ELECTRON GAS

In this chapter we present a brief introduction to the two-dimensional electron gas in GaAs/$Al_x Ga_{1-x}$As heterostructures: its formation, the calculation of its eigenstates and the sample preparation.

The occurrence of the quantized Hall effect is restricted to conducting systems with a two-dimensional character. Such systems are obtained by confining the charge carriers to some kind of potential well. These carriers can be electrons or holes, but we will restrict ourselves to the two-dimensional electron systems. Because the electrons move almost freely in the plane of confinement, which we name the xy-plane, these systems are usually called two-dimensional electron gases. The confining potential, which depends on the z-direction, can be achieved in several ways.

Regarding the two-dimensional electron gases in semiconductors, the most commonly used structures are the GaAs/$Al_x Ga_{1-x}$As heterostructure and the Si-MOSFET, not the least because of their availability. The GaAs/$Al_x Ga_{1-x}$As heterostructure offers major advantages. It has both the higher mobility and the lower effective mass; therefore quantization effects occur at lower magnetic fields. In addition it shows the linear electro-optic effect, which enables us to perform contactless measurements of the potential distribution. All measurements presented in this thesis are performed on these heterostructures.

A schematic drawing of the various layers of such a heterostructure is shown in Fig. 2.1. The heterostructure in its simplest form consists of a Si-doped (n-type) $Al_x Ga_{1-x}$As layer on top of a GaAs layer, which is usually slightly p-type due to residual background impurities. As a consequence of the difference in work function of both materials, electrons flow from the $Al_x Ga_{1-x}$As to the GaAs. Due to this charge transfer electric fields build up until the Fermi level ϵ_F is equal throughout the entire device. This results in a potential well at the interface of the GaAs and $Al_x Ga_{1-x}$As acting as the confining potential of the two-dimensional electron gas. If the well is deep enough, it contains a two-dimensional electron gas. A more

elaborate description of this process will be presented after a discussion of the other layers which are shown in Fig. 2.1, where also typical dimensions of the structure are indicated.

At low temperatures ($\approx$ 4 K) the donors in the $Al_xGa_{1-x}As$ layer are the main scattering source. Since the two-dimensional electron gas and the donors are spatially separated from each other, the mobility of the two-dimensional electron gas is enhanced above the bulk value. A further enhancement of this mobility can be achieved by inserting an additional undoped $Al_xGa_{1-x}As$ spacer layer in between the GaAs and Si-doped $Al_xGa_{1-x}As$ layer. In this way the distance between the electrons in the two-dimensional electron gas and the charged donors in the doped $Al_xGa_{1-x}As$ is enlarged. In Fig. 2.1 also a GaAs cap layer is shown, which prevents the Al in the $Al_xGa_{1-x}As$ from oxidation. The whole structure is grown on a GaAs substrate by means of e.g. an MBE (molecular beam epitaxy) or MOCVD (metal organic chemical vapour phase deposition) technique. We do not discuss these growth techniques here.

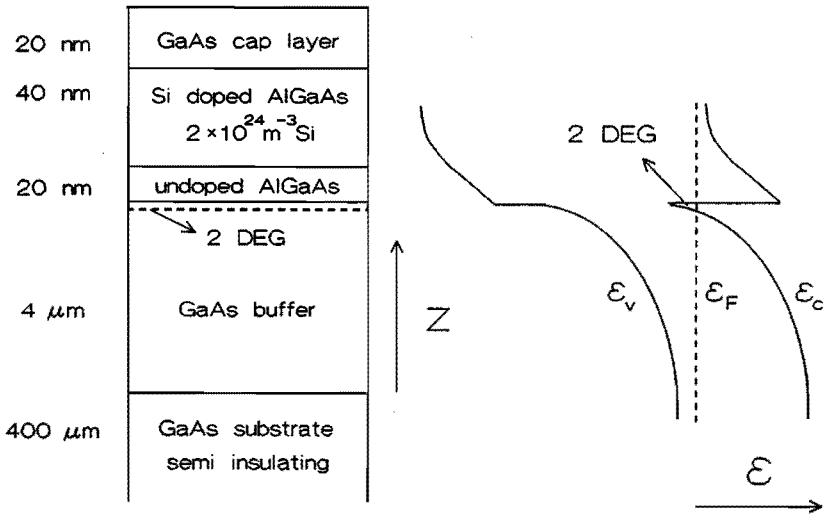**Fig. 2.1** *Schematic drawing of the various layers in a $GaAs/Al_xGa_{1-x}As$ heterostructure. The indicated dimensions should be regarded as typical values. On the right the energy band diagram of the $GaAs/Al_xGa_{1-x}As$ heterostructure is drawn, with the position of the two-dimensional electron gas (2 DEG) indicated. The indices c and v stand for conduction and valence band respectively.*

Note that, due to the confinement of the electrons, the bottom of the conduction band near the $GaAs/Al_xGa_{1-x}As$ interface as drawn in Fig. 2.1 is no longer associated with the presence of electron states at that specific energy. The calculation of the energies is usually carried out within the so-called effective mass approximation. In this approximation the details of the lattice potential due to the ions at the lattice sites are accounted for by the assignment of an effective mass m^* to the conduction electrons. In this way the complexity of the problem is reduced considerably. The Poisson equation (Eq. (2.1)) has to be solved self-consistently with the Schrödinger equation (Eq. (2.2)):

$$\partial^2 V/\partial x^2 + \partial^2 V/\partial y^2 + \partial^2 V/\partial z^2 = -q(x,y,z)/\kappa(z), \qquad (2.1)$$

$$(-\hbar^2/2m^* \ \partial^2/\partial z^2 + U_0(z) + U_c(z) + U_{ex}(z)) \ \phi_i(z) = \epsilon_i \phi_i(z), \qquad (2.2)$$

where U_0 accounts for the conduction band discontinuity, $U_c = -eV$, with e the elementary charge, V the electrostatic potential, U_{ex} an exchange correlation potential, ϕ the z-dependent part of the wave function, $q(x,y,z)$ the charge density, and κ the dielectric constant. Note that the electrostatic potential is not a constant, but adjusts itself to a value such that the Schrödinger and Poisson equation are obeyed simultaneously. The first two terms in Eq. (2.1) are zero in case of a homogeneous sample, since in that case q does not depend on x and y. This charge includes, of course, the electrons in the two-dimensional electron gas, the positive donors in the doped $Al_xGa_{1-x}As$ layer and the negatively charged acceptors in the GaAs layer. As a result of the calculation the allowed energy states in the potential well are quantized, with energy eigenvalues ϵ_i $(i = 0, 1, ..)$ associated with the confinement in the z-direction. All states belonging to the same eigenvalue ϵ_i constitute an (electric) subband. In contrast, a continuum of energy eigenvalues $\epsilon(k)$ is associated with the motion in the xy-plane. This energy can be written as $\epsilon(k) = \hbar^2 k^2/2m^*$, with $\hbar = h/2\pi$, h Planck's constant and k the magnitude of the wave vector in the xy-plane. The distribution of the electrons across the different subbands depends on the density of states $D(\epsilon)$ and, through the Fermi-Dirac distribution function, also on the temperature T.

In order to be able to measure the characteristic properties of the two-dimensional electron gas, the wafer, as grown, needs further processing. A structure must be defined and contacts must be made to the electron gas. Two kinds of

structures are generally used, the Hall bar and the Corbino disc, see Fig. 2.2. These structures are photolithographically defined and mesa-etched. The contacts are made either by alloying AuGeNi films or small dots of In or Sn into the sample until they make contact to the electron gas. For Corbino structures AuGeNi contacts must be used, because in this way one can make contact to the entire periphery of these structures.

After these processing steps it is advisable to check the quality of both the contacts and the sample. The contacts must be ohmic and have a low resistance. Further, if possible, the homogeneity of the sample must be checked, see also chapter 4. If these conditions are met we can perform a quantized Hall measurement, which we will describe in the next chapter.
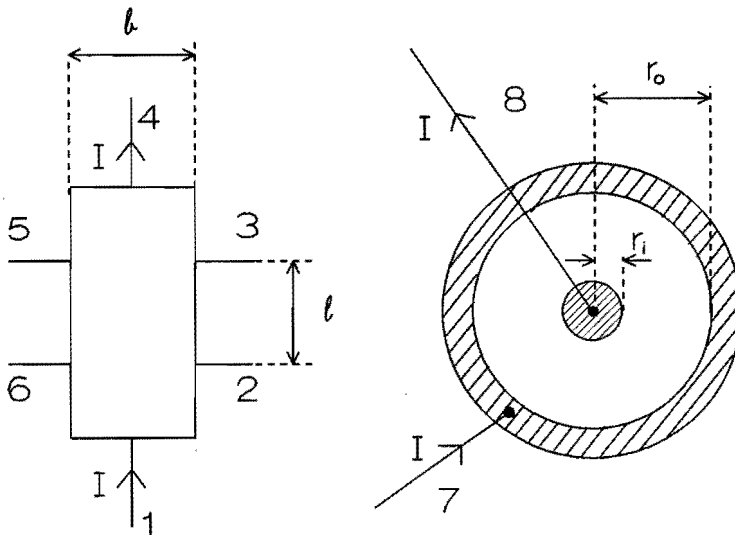
Fig. 2.2 *Hall bar (left) and Corbino disc (right). Usually a current I is sent through the device and the resulting voltages V_{ij} are measured in order to determine the various parameters of the two-dimensional electron gas.*

CHAPTER 3

THE QUANTIZED HALL EFFECT – EXPERIMENT AND MODELS

3.1 About this chapter

The aim of this chapter is to provide the reader some background information concerning the quantized Hall experiment and its models. The information supplied should suffice to understand the remaining part of this thesis, where we present and discuss our own experiments on the quantized Hall effect.

3.2 The experiment

The quantized Hall effect is usually measured with a Hall bar structure, like the one depicted in Fig. 2.2. The sample, which contains a two-dimensional electron gas, is cooled down to a temperature of a few kelvin and a current I is sent through the contact pair 1 and 4. Next, a magnetic field B is applied perpendicular to the structure and the voltages across the different pairs of contacts are determined as a function of this magnetic field. Along the length of the structure the so-called Shubnikov-de Haas voltage is measured, which oscillates as a function of magnetic field. Across the width of the structure a Hall voltage with accurately quantized plateaus is measured, the quantized Hall effect. This is clearly visible in Fig. 1.1. The ratio of the Hall voltage and the current, the Hall resistance, is accurately quantized to the value h/ie^2, with $i = 1, 2, 3, ...$

In the above we have tacitly assumed that we use a Hall bar structure which is much longer than wide, with the voltage probes separated from the current contacts by a distance much larger than the width of the sample. This geometry leads to a current distribution which is parallel to the edges of the sample at the position of the voltage probes. This has the advantage that no mixing of the Shubnikov-de

Haas voltage and the Hall voltage occurs. This will be clear if we recall the definition of the resistivity tensor ρ and its inverse the conductivity tensor σ:

$$
\begin{aligned}
E_x &= \quad \rho_{xx} j_x + \rho_{xy} j_y, & j_x &= \quad \sigma_{xx} E_x + \sigma_{xy} E_y, \\
E_y &= -\ \rho_{xy} j_x + \rho_{xx} j_y, & j_y &= -\ \sigma_{xy} E_x + \sigma_{xx} E_y,
\end{aligned}
\qquad (3.1)
$$

with j the current density and E the electric field. In the above definition an isotropic two-dimensional electron gas is assumed. If the y-direction is the direction of the current in Eq. (3.1) and j_x is zero, it is easy to derive that

$$
\begin{aligned}
\rho_{xx} &= (V_{23}/I)(b/l), \\
\rho_{xy} &= V_{35}/I,
\end{aligned}
\qquad (3.2)
$$

with V_{ij} the potential difference across the contacts i and j. From these equations it is obvious that the Shubnikov-de Haas resistivity ρ_{xx} and the Hall resistivity ρ_{xy} can be measured separately. Note, however, that the orientation of the coordinate system is of no importance, it is only the easiest way to orient one of the axes along the boundary of the sample.

The astonishing property of the quantized Hall effect is the preciseness of the quantization of ρ_{xy} to the value h/ie^2. This value does not depend on specific sample properties, like details of the scattering mechanism or electron concentration, and thus seems to be a fundamental property of the two-dimensional electron gas. This fact has led to the development of a variety of models to describe the quantized Hall effect. In the next sections we will present and discuss some of these models.

3.3 Electrons in a high magnetic field – the localization model

Classically an electron in a two-dimensional electron gas subjected to a perpendicular magnetic field will move in cyclotron orbits with angular frequency $\omega_c = eB/m^*$. It can be shown that in the absence of scattering and under the

influence of an electric field the drift velocity v_d of the centre of the cyclotron orbit is equal to

$$v_d = E \times B / B^2. \tag{3.3}$$

Thus the electron drifts perpendicular to the electric field along equipotential lines, and hence $\rho_{xx} = 0$ and $\rho_{xy} = B/ne$, with n the electron concentration. This can be verified from the force balance between the Lorentz force and the electric force; see also section 5 of this chapter.

To incorporate quantization a quantum mechanical treatment is necessary. The solution of the Schrödinger equation of a two-dimensional electron gas in a magnetic field[12] leads to quantized energy eigenvalues

$$\epsilon_N = (N + \tfrac{1}{2}) \hbar \omega_c, \tag{3.4}$$

with $N = 0, 1, \dots$. Note that we only deal with the lowest electrical subband. Every level ϵ_N has a degeneracy of $2eB/h$ and is called a Landau level, see Fig. 3.1(a).

The magnetic field lifts the degeneracy of the spin up and spin down level, see Fig. 3.1(b). Every spin level has a degeneracy of eB/h instead of the earlier $2eB/h$. Eq. (3.4) becomes $\epsilon_{N,s} = (N + \tfrac{1}{2})\hbar\omega_c + sg^*\mu_B B$, with $s = \pm\tfrac{1}{2}$, the spin quantum number, g^* the effective g-factor and μ_B the Bohr magneton ($= e\hbar/2m$, m the rest mass of the electron). The spin splitting is smaller than the Landau splitting by a factor $g^*m^*/2m$ ($m^*/m = 0.0667$ for GaAs), so it will be observable in the transport coefficients only at higher magnetic fields. But care has to be taken, since the g-factor depends on filling factor and magnetic field[13].

The discrete Landau levels are broadened by scattering. Usually a Gaussian broadening is assumed with a characteristic width Γ, see Fig. 3.1(c). The exact shape, however, is still a subject of controversion in literature[14]. If the level broadening is smaller than the Landau level spacing ($\Gamma < \hbar\omega_c$) and the temperature is sufficiently low ($k_B T \ll \hbar\omega_c$, with k_B the Boltzmann constant) the quantization can be observed in the transport coefficients. The first condition can also be formulated as $\mu B > 1$, with the mobility $\mu = e\tau/m^*$, τ the scattering time. This means classically that, on the average, the electron performs at least one cyclotron revolution between two scattering events.

The number of Landau levels below the Fermi level depends on B, because the electron concentration is fixed and the degeneracy of the Landau levels depends on magnetic field. If the Fermi level is situated at a maximum of the density of states, the scattering will show a maximum. At a minimum of the density of states it will show a minimum. If the magnetic field is varied, the Landau levels will move through the Fermi level and thus the quantities ρ_{xx} and σ_{xx} will oscillate as a function of the magnetic field. The Hall resistivity is hardly affected by the quantized density of states, since it depends on the total number of electrons and simply increases with magnetic field.

Now consider the case where the Fermi level is centred between two Landau levels which are completely separated. The density of states at the Fermi energy is completely zero in this case. Suppose that there are i Landau levels below the Fermi energy and suppose that there is no thermal activation of electrons from Landau
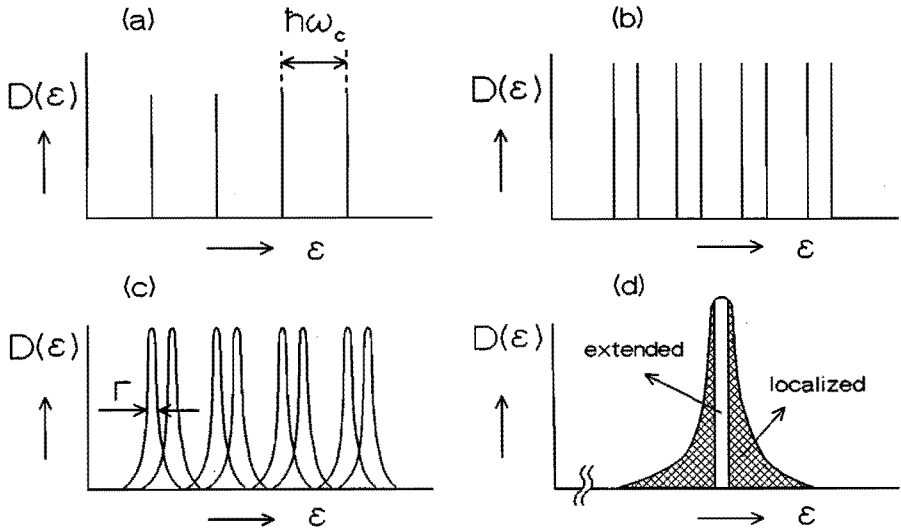

Fig. 3.1 *Density of states in the presence of a magnetic field (a). If the magnetic field is sufficiently high the spin splitting becomes observable (b). The Landau levels broaden due to scattering (c). Due to the scatterers, combined with the magnetic field, the tails of the Landau levels become localized (d).*

level i to Landau level $i+1$. If all these conditions are satisfied the i Landau levels are completely filled and no scattering occurs. Thus ρ_{xx} is zero and ρ_{xy} equals $B/(e\ ieB/h) = h/ie^2$. So the Hall resistivity has the correct quantized value. However, this quantized value is only obtained for one specific value of the magnetic field, no plateau occurs. Also the resistivity ρ_{xx} rapidly increases with changing magnetic field and no broad minimum is predicted.

In order to explain plateaus the keyword 'localization' comes into play. As we have seen earlier, the electrons drift perpendicular to the electric field. It is possible that a charge in the neighbourhood of the two-dimensional electron gas creates a hill or a valley in the electrostatic potential as a function of position. As a consequence there exist closed equipotential loops around such a hill or valley. A particle which drifts along such an equipotential is said to be localized. Note that this can be the case both around negative and positive charge, in contrast to the so-called extended states, which can move freely through the sample from one current contact to the other.

In the description presented above the localized state has a macroscopic character. The cyclotron orbit is assumed to be small with respect to the potential hill or valley, otherwise it is impossible to speak in terms of a drifting cyclotron orbit. The other extreme is a rapidly fluctuating potential confined to a small area, e.g. the delta scatterer, which is infinitely small but has an infinitely high scattering potential. This delta scatterer can also bind or localize an electron[5], see section 3.5.

Concerning the energy of the localized states we can state that due to the Coulomb interaction they have a lower (around a positive charge) or higher (around a negative charge) energy than the extended states. So the localized states reside in the tails of the Landau levels, the centre is extended, see Fig. 3.1(d).

The quantized Hall effect is now usually 'explained' as follows:
If the Fermi level is in a localized region and the temperature is sufficiently low there is no scattering between the extended states and ρ_{xx} shows a minimum of nearly zero as long as the Fermi level is within this region. Thus ρ_{xx} is nearly zero within a certain range of magnetic fields. There is also no change in the properties and number of extended states if one electron is added to the system (and thus to the localized states), and hence ρ_{xy} remains constant. Note that this last argument uses a change of n, not B. In case B is varied the number of extended states has to be adapted in order to keep the ratio $B/n_{ext}e$ constant, with n_{ext} the number of extended states. If $n_{ext} \neq eB/h$, however, the ρ_{xy} value will not have the correct

quantized value (if $\rho_{xy} = B/n_{ext}e$). Furthermore the picture of Fig. 3.1 yields no information about the spatial position of the extended and localized wave functions, but shows some kind of a spatial average. We will comment on these problems in the next sections.

3.4 The gauge argument

Laughlin was the first to explain the quantized Hall effect by using a so-called gauge argument[8]. Halperin made a slight extension and modification to the model, which we will discuss below[9].

Imagine a ring shaped structure, like a Corbino disc, consisting of a disordered region surrounded by boundaries of a perfect two-dimensional electron gas. It is assumed that these boundaries are at integer filling factor and thus have $\rho_{xy} = h/ie^2$ and $\rho_{xx} = 0$. The ideal properties of the boundaries are used in the following to make statements about the disordered region (with localization).

If the flux Φ threading the inner loop of the disc is changed by a flux quantum h/e a current will flow in the radial direction. This can be understood in terms of Maxwell's equation $d\Phi/dt = \oint E \cdot dl$, which implies that a flux change induces a tangential electric field E. The magnitude of the outward flowing current $I = 2\pi r j_r$, with r the radius, corresponds to this field. If the flux Φ changes by h/e in a time interval Δt this leads to $d\Phi/dt = h/e\Delta t = \rho_{xy} 2\pi r j_r$. Since the induced current can be written as $\Delta Q/\Delta t$, with ΔQ the transported charge, we get $h/e\Delta t = (\Delta Q/\Delta t)(h/ie^2)$ or $\Delta Q = ie$. Thus, due to the flux change for every Landau level one electron is transferred. The localized states do not enclose the loop and are not affected by the flux change. As a consequence their energies and wave functions are not changed. Therefore the so-called gauge argument can be applied to the extended wave functions. The argument states that the integer number of flux quanta can be removed by an appropriate gauge transformation and so the resulting wave functions of the extended states are identical to the ones we started with. The net result is that every extended state is shifted into its neighbour state and a total of i electrons is transferred from one edge to the other.

Thus we can conclude that the imperfect region of localized states does not affect the number of electrons transferred and hence a macroscopic measurement of ρ_{xy} results in the value h/ie^2. Note, however, that this model does not explain the occurrence of a plateau.

3.5 The single scatterer and percolation models

Prange presents in his paper[5] an exact calculation of the influence of a delta function impurity on the properties of a two-dimensional electron gas. It turns out that an electron state develops which is localized on the impurity. However, the remaining mobile electrons passing the impurity carry an extra current which exactly compensates for the loss of current by the localized electron. So the Hall resistance is still exactly quantized.

The underlying physics of the mathematically quite involved calculations of Prange have been made accessible to 'experimentalists' by Hansen[6].

Consider the case of an infinitely long two-dimensional electron gas with width L_x in the x-direction subjected to a perpendicular magnetic field. An electric field E_x in the x-direction is applied. We will first treat the impurity free case with an integer number i of Landau levels filled. The net force on all electrons has to be zero. Thus, if we consider a piece of the infinitely long structure with length L_y, the Lorentz force $-BIL_y$ (with I the current) has to be equal to the electrostatic force $L_xL_y(ieB/h)E_xe = L_y(ie^2/h)BV_H$, with V_H the Hall potential. If an impurity is added to the system a bound state can appear. The extra forces F_{ib} and F_{im} (the force of the impurity on the bound and mobile states respectively) will have to be included in the force balance equation:

$$L_y(-BI + V_Hie^2B/h) + F_{ib} + F_{im} = 0. \tag{3.5}$$

It is clear that $F_{ib}+F_{im}$ has a certain finite value. Since Eq. (3.5) has to be valid irrespective of L_y, both the expression in brackets and the sum of the forces acted by the impurity must be zero. So $V_H = h/ie^2$ despite the presence of localization.

What is the physical picture behind? The electric field pulls at the bound electron. The impurity pulls it back with an equal but opposite force. The bound state becomes polarized and the impurity acts with an opposite force on the mobile electrons (as $F_{ib} = -F_{im}$). This force is exactly the force needed to compensate for the loss of one mobile electron contributing to the current. So in the vicinity of a localized state the electrons will move faster, they are speeded up by an extra electric field. The situation is more or less comparable to an obstruction in a river with the water squeezed around. Since no restrictions are imposed on the shape of the impurity potential, the same arguments hold for an arbitrary number of impurities. However, no plateaus are predicted! Again it is only predicted that $\rho_{xy} = h/ie^2$ at integer filling factor, irrespective of the presence of localized states.

Related, but only applicable to situations with long range inhomogeneities, are the so-called percolation models of which we describe below the models of Woltjer and Luryi.

In the model of Woltjer[4] ρ_{xy} and ρ_{xx} are calculated from a theoretical expression derived by Ando et al[12]. This expression results in $\rho_{xy} = h/ie^2$ and $\rho_{xx} = 0$ at zero temperature and integer filling factor. No plateaus in ρ_{xy} occur however within Ando's model. In order to obtain plateaus Woltjer incorporates a gradient in the electron concentration across the width of the sample. In this case a range of magnetic fields exists at which there is a percolating path with integer

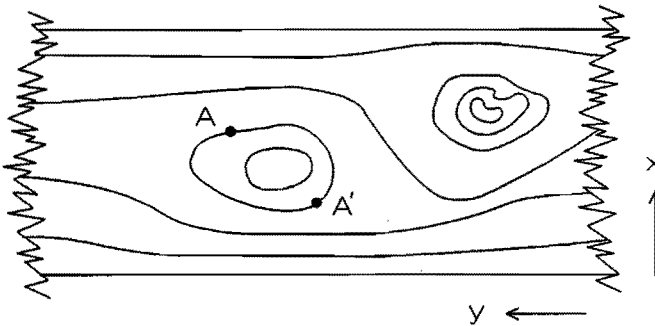**Fig. 3.2** *Example of the equipotential lines across the sample, according to Luryi[3]. Indicated are two points A and A', which are on the same equipotential. The whole region enclosed by this equipotential becomes localized in a magnetic field.*

filling factor (in this case a straight line) from current contact to current contact. Since for this path ρ_{xx} is nearly zero at low temperatures, most of the current flows along this path. The measured 'apparent' ρ_{xy} is some average over the sample and shows the quantized value over the range of fields for which this path exists.

The model of Luryi[3] looks similar and assumes two-dimensional macroscopic inhomogeneities in the potential distribution to be present, like in Fig. 3.2. Luryi argues that integration over the electric field from A to A' does not result in any potential difference, because A and A' are situated on the same equipotential. The region within the equipotential on which A and A' are situated is localized. In other words, it would be possible to cut these regions of localized states out of the sample, without changing the Hall potential. Plateaus will occur over the range of magnetic fields where the percolating paths have integer filling factor. Such a range exists due to the fact that the potential hills and valleys act as a kind of buffer, see also section 4.2.

3.6 Edge states

In the Büttiker model[7] contacts act as electron reservoirs. At zero temperature a contact with Fermi level ϵ_F can inject electrons up to this Fermi energy. Also electrons impinging on a contact can be absorbed by the contact, irrespective of their energy. A contact is called ideal if it absorbs all electrons impinging on that contact and fills all the empty states in the sample up to ϵ_F by injecting electrons.

First consider the one-dimensional conductor sketched in Fig. 3.3, with two ideal contacts attached to both ends and calculate its conductance. The contacts are at ϵ_{F1} and ϵ_{F2} respectively. Further assume scattering to be absent in the structure. This implies that all electrons which are injected at one contact end up at the other contact, in other words the transmission probability is equal to one. It is clear that the conductance of the two-terminal device is proportional to the number of electrons with energies in between ϵ_{F1} and ϵ_{F2} times their velocity. The motion of electrons at lower energies cancels. Hence the conductance can be calculated from

the electrons between ϵ_{F1} and ϵ_{F2} alone. The total current can be written as $I = nev_g$, with v_g the group velocity

$$v_g = 1/\hbar \, d\epsilon/dk, \tag{3.6}$$

and n the concentration of electrons between ϵ_{F1} and ϵ_{F2}. The calculation of the conductance is now rather straightforward. In an energy interval $\Delta\epsilon$ around ϵ_F there are $D(\epsilon=\epsilon_F)\Delta\epsilon$ electrons, with $D(\epsilon) = (dn/dk)/(d\epsilon/dk)$. It is clear that the terms $d\epsilon/dk$ in v_g and $D(\epsilon)$ cancel in the product $I = nev_g$. This peculiarity leads to $I = (\epsilon_{F2}-\epsilon_{F1})e/h$, where $dn/dk = 1/2\pi$ is inserted. The value $1/2\pi$ can be derived from the particle in a box problem. If a voltage measurement across the two contacts is performed a voltage $V = (\epsilon_{F2}-\epsilon_{F1})/e$ is measured. The ratio of this voltage and the current leads to a conductance of e^2/h. If i one-dimensional subbands are present this changes into $I = V\,ie^2/h$. So the conductance (I/V) of the one-dimensional structure is quantized in units e^2/h.
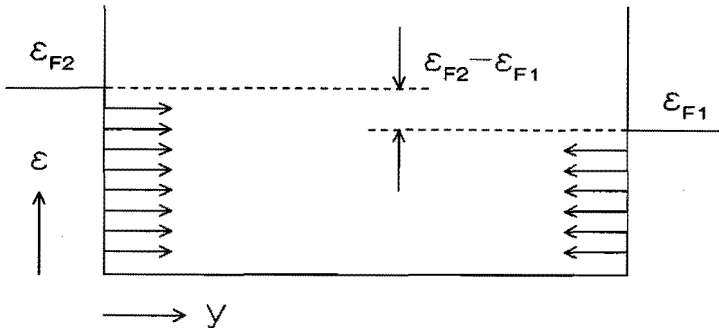

Fig. 3.3 *One-dimensional conductor with two contacts at ϵ_{F1} and ϵ_{F2} respectively. No scattering is supposed to occur. The net current is determined by the states in between ϵ_{F1} and ϵ_{F2}.*

The beauty of the Büttiker formalism is that the same arguments can be applied to the quantized Hall effect in two–dimensional systems. This is because in a magnetic field the electron wave functions also have a one dimensional character:

$$\Psi_N(x,y) = e^{iky} \, g(x-x_0,N), \tag{3.7}$$

with $g(x-x_0,N)$ the solution of the harmonic oscillator problem centred around x_0 with characteristic length

$$l = (\hbar/eB)^{\frac{1}{2}}, \tag{3.8}$$

the magnetic length. The centre x_0 is related to the wave number k in Eq. (3.7) via

$$x_0 = kl^2. \tag{3.9}$$

In this case the Landau levels of the two–dimensional system play the role of the different subbands in the one–dimensional system. It can be proved in a similar way that the Hall resistance is quantized in units h/ie^2, if the transmission probability is equal to one. The only difference is that the position x_0 of the states with different k values is the same in the one–dimensional case, but depends on k for the quantized Hall case.

Originally Büttiker sketched the following situation: The two–dimensional electron system is situated in a potential landscape with hills and valleys. At the edges the confining potential steeply increases in order to keep the electrons within the sample. Hence there will always exist an equipotential line from contact to contact along the edges. Along this equipotential line there exists an extended state, the interior will be localized. The energies of the Landau levels in this confining potential differ from those calculated earlier (Eq. (3.4)). Due to the confinement the Landau levels bend upward at the edges, like indicated in Fig. 3.4. This bending introduces a non–zero group velocity of the electrons at this position, see Eq. (3.6). At one edge the electrons move to the left, at the other to the right, because the sign of the slope of the energy as a function of position is opposite. The states with non–zero velocity can be compared with the classical so–called skipping orbits.

Now the picture of the quantized Hall effect like it was originally depicted by Büttiker can be drawn, see Fig. 3.4. If the Fermi level is situated in between the 'bulk' Landau levels the net contribution to the current is given by the electrons at the edge with the higher Fermi energy only. These so-called edge states can scatter, but due to the presence of the magnetic field their group velocity will always be directed in the same direction. So there is no backscattering and the transmission probability is one. The transmission probability will start to differ from one in case the Fermi level is situated within a 'bulk' Landau level. In this case an electron can move from one edge to another through subsequent scattering events. Thus not all electrons injected at one contact arrive at the other contact, some might return via the other edge, and the quantization vanishes.

Backscattering may also occur at high current levels. If $\epsilon_{F2}-\epsilon_{F1} > \hbar\omega_c$ there will be scattering from the upmost Landau level to the other edge. This limits the range of currents at which the Büttiker model can be valid to a maximum value of about 100 nA under typical experimental conditions. Note that usually higher currents are applied. At high currents one always has to include the effects of the
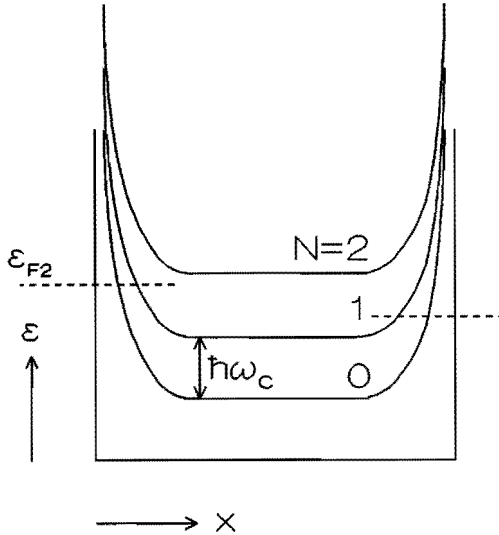

Fig. 3.4 *Landau levels in the presence of a confining potential. At the edges the confining potential causes the Landau levels to deviate from their 'bulk' value.*

electric field in order to be able to describe the quantized Hall effect correctly. It is easy to make an extension to this more general situation, see Fig. 3.5. Due to the electric field the electrons obtain an extra drift velocity $v_d = E_x/B$. It can be shown that this drift velocity is already accounted for by Büttikers group velocity $v_g = 1/\hbar\ (d\epsilon/dk) = 1/\hbar\ (d\epsilon/dx_0)(dx_0/dk)$. The factor dx_0/dk can be obtained from Eq. (3.9) and is equal to l^2. If an homogeneous Hall field is present this leads to an extra energy term $eE_x x_0$. So $d\epsilon/dx_0 = eE_x$ and substitution leads to $v_g = E_x/B = v_d$. This picture has been visualized in Fig. 3.5. The electrons which are situated on the line segments of Fig. 3.5 which have been indicated by 'loc' cancel with respect to their contribution to the current. It is easy to imagine that the indicated regions are just the part of the sample from A to A' in Fig. 3.2. Thus the parts that cancel are (comparable to) localized states. Also the extended states can be taken the same as those of Luryi and thus these models become very similar.
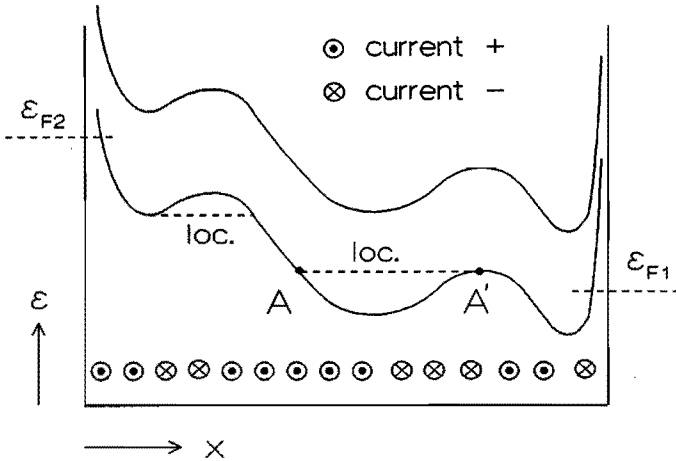

Fig. 3.5 *Büttiker model generalized to the situation where currents flow in the interior of the sample. The states indicated by 'loc' and the dashed lines can be regarded as localized, the others are extended. A situation comparable to that of Luryi occurs. The region $A - A'$ can e.g. be compared to that of Fig. 3.2.*

CHAPTER 4

INHOMOGENEITIES AND THEIR INFLUENCE
ON THE CURRENT DISTRIBUTION
IN THE QUANTIZED HALL EFFECT

4.1 Introduction

In solid state physics inhomogeneities are very often made responsible for differences between experiment and theory, if one cannot confirm their presence by an independent experiment or if one cannot calculate their influence.

The same situation applies to the quantized Hall effect in two-dimensional electron gases. We have already mentioned the models of Woltjer and Luryi in section 3.5, where the quantized Hall effect is thought to be due to spatial variations in the electron concentration. More generally the whole picture of localization is strongly interwoven with these inhomogeneities.

In section 4.2 we present numerical calculations on inhomogeneous two-dimensional electron gases under quantized Hall conditions. These calculations show what the influence of inhomogeneities might be and how rigorously spatial variations must be taken into account for explaining the experimental observations. The current distribution which is calculated there is the externally imposed current. At the end of section 4.2 we also discuss the difference between the local current density caused by internal electric fields, which can be present due to inhomogeneities, and the current density which is imposed by the external electric field. This topic is of special interest for the spatially resolved potential measurements which we present in chapter 5.

In section 4.3 we explain why we think inhomogeneities are present. Further we comment on some methods, which exist to determine these. It turns out that only very little is known about the subject of inhomogeneities.

4.2 How an inhomogeneous electron concentration influences the current distribution in the quantized Hall effect: a model for 'dynamic' localization

We consider inhomogeneities in the electron concentration of at most a few percent. Variations of 1 % normally have only a small influence on the current distribution. However, we will show that when a magnetic field is applied, the current distribution can be strongly modified in spite of the very small variations in electron concentration.

First, we clarify why these small inhomogeneities can have such a strong influence. Next, we consider their role in the occurrence of the quantized Hall effect, the asymmetry in the high magnetic field Shubnikov-de Haas effect and structure in Shubnikov-de Haas minima.

Consider the situation in which two semi-infinite two-dimensional electron gases are connected to each other, see Fig. 4.1. Both regions (1, 2) have their own electron concentration n and resistivity tensor components ρ_{xx} and ρ_{xy}. The electric field and the current density are connected via $E = \rho j$. The system obeys the equation

$$\text{div } j = 0. \tag{4.1}$$

It can be shown that because of the translational symmetry along the x-axis $\partial j_x / \partial x = 0$. Thus with Eq. (4.1) it follows that $\partial j_y / \partial y = 0$ and thus $j_{y1} = j_{y2} = j_y$. At the boundary $E_{x1} = E_{x2}$. Therefore we can derive that at this boundary

$$j_y(\rho_{xy1} - \rho_{xy2}) = \rho_{xx2}\, j_{x2} - \rho_{xx1}\, j_{x1}. \tag{4.2}$$

This means that the difference in Hall voltage caused by j_y in regions 1 and 2 has to be fully compensated for by currents in the x-direction. If we apply a magnetic field of e.g. 1 T and if we assume an electron mobility of $100\,\mathrm{m^2/Vs}$ we get $\rho_{xy}/\rho_{xx} = 100$. If we assume $\rho_{xx1} \approx \rho_{xx2}$ Eq. (4.2) tells us that a difference between ρ_{xy} in regions 1 and 2 of 1 % results in almost equal currents j_x and j_y. But within a quantized Hall plateau where ρ_{xy}/ρ_{xx} can easily be 10^7, j_x turns out to be five orders of magnitude larger than j_y. In an ordinary Hall bar this j_x has a tremendous

influence on the current distribution and hence on the voltages measured along the Hall bar structure, which we will show later.

After this rather qualitative discussion we will now go into a more detailed calculation. We chose for a numerical approach of the calculation of the current distribution. Apart from Eq. (4.1) a second equation is involved:

$$\text{rot } \boldsymbol{E} = \boldsymbol{0}. \tag{4.3}$$

If we apply $\boldsymbol{j} = \sigma \boldsymbol{E}$ to Eq. (4.1) and use Eq. (4.3) and $\boldsymbol{E} = -\text{grad } V$ one can deduce that

$$
\begin{aligned}
\sigma_{\text{xx}} \left(\partial^2 V / \partial x^2 + \partial^2 V / \partial y^2 \right) \quad & + \left(\partial \sigma_{\text{xx}} / \partial x - \partial \sigma_{\text{xy}} / \partial y \right) \partial V / \partial x \\
& + \left(\partial \sigma_{\text{xy}} / \partial x + \partial \sigma_{\text{xx}} / \partial y \right) \partial V / \partial y = 0.
\end{aligned} \tag{4.4}
$$

The system we want to study is a Hall bar structure. However we are only interested in effects caused by inhomogeneities, and not in contact or boundary effects. Therefore we apply periodic boundary conditions in the y-direction. The two
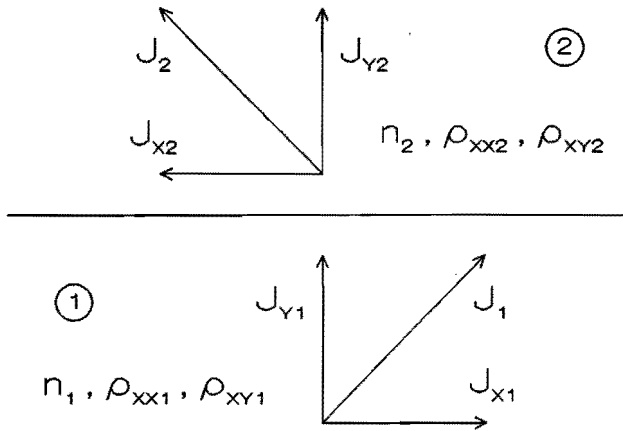

Fig. 4.1 *Two homogeneous regions 1 and 2 with different electrical properties. The two regions are connected along the x-axis. A current j_y flows upward. It is demonstrated in the text that a magnetic field can cause currents j_x to appear which are much larger than j_y.*

other boundaries of the periodic rectangular structure are governed by the boundary condition $j_x = 0$.

In case of a homogeneous sample the current distribution can very easily be derived from Eq. (4.4). In this case the current will be distributed homogeneously if $\sigma_{xx} \neq 0$, as we will show in chapter 5, where we also consider the special case of $\sigma_{xx} = 0$.

We solved Eq. (4.4) numerically under the boundary conditions discussed above. To this end we applied a 70x70 discretisation grid, resulting in a 4900x4900 sparse matrix equation. The accuracy of the calculations is governed by the number of discretisation points compared to the magnitude of the inhomogeneities. We carefully checked that the numerical errors in this work rested within acceptable limits.
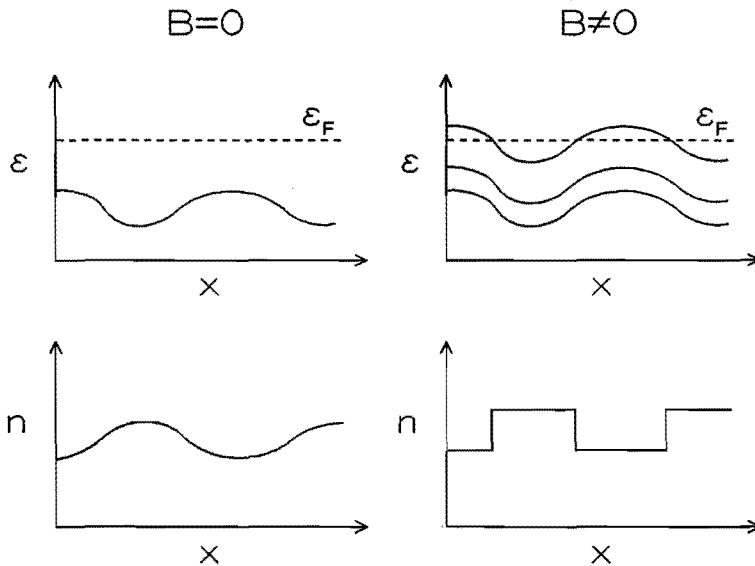

Fig. 4.2 *A schematic view of an inhomogeneous ϵ-distribution. Shown is the situation at zero magnetic field (left) and non-zero magnetic field (right). A smooth electron distribution is possible in case B = 0. If B ≠ 0 the electron concentration shows a jump at the position where the Fermi level crosses a Landau level.*

The results of our calculations which we present in the following are obtained on two types of model systems. The one has a fixed electron distribution as a function of position, the other a fixed potential distribution or potential landscape which is filled with electrons up to the Fermi level. These two are equivalent at zero magnetic field, see Fig. 4.2. If a magnetic field is applied the situation gets more complicated. Landau levels occur, which means that in the case n is constant abrupt steps in the Fermi energy appear where it moves from one Landau level to another. This situation results in a redistribution of charge until a voltage difference across the redistributed charge is obtained which equals the step in Fermi energy. It has been shown[15] that this can result in charge redistributions up to 1 μm. The charge redistribution strongly favours Landau levels to be completely filled or completely empty. This is exactly what one obtains within the model with a fixed potential distribution. Within this model the charge distribution depends on magnetic field or Fermi energy. When the inhomogeneities are of the order of the charge redistribution length (1 μm) it is a better description than the model which assumes a constant charge carrier distribution. In case of long range inhomogeneities the fixed n distribution is the better approximation since the region in which the charge redistribution takes place is small compared to the range of the inhomogeneities. We want to stress, however, that neither of the two models is perfect.

First, we present calculations on a system with a fixed electron distribution which is inhomogeneous in two directions. Our results indicate that interesting localization effects occur. Consider the case with

$$n(x,y) = n_0(1 + 0.005 \cdot \sin(\pi x) \cdot \sin(2\pi y)) \qquad 0 \leq x \leq 1 \qquad (4.5)$$
$$\rho_{xx} = (10^{-3} + 5 \cdot 10^{-1} \cdot (n - n_0 B/B_0)^2)/n_0 e \mu_0$$
$$\rho_{xy} = B/ne.$$

In these equations we have chosen values which are in agreement with the experiments. For example ρ_{xx} is chosen such that it shows a minimum around a magnetic field $B = B_0 n/n_0$, with $n_0 = 5 \cdot 10^{15}$ m^{-2} and $B_0 = 5$ T. These parameters correspond to a filling factor 4 around a magnetic field of 5 T. We chose $\mu_0 = 10$ m^2/Vs. The electron distribution is chosen such that there is a path across the sample with a constant electron concentration. We calculated the current and voltage distribution around 5 T in the entire sample. From this we took the potentials at specific points, which may be considered as voltage probes, and

calculated the 'apparent' values of ρ_{xy} and ρ_{xx} which one would obtain from an electrical transport measurement; see Fig. 4.3. These calculated values represent averages of local resistivities. Since we measure resistances and not resistivities we introduce the quantities R_{xy} and R_{xx} respectively. It is clear that there is some structure visible in R_{xy} but that there is certainly no plateau present. The minimum in R_{xx} we observe is rather sharp.

If we replace $n(x,y)$ in Eq. (4.5) by

$$n(x,y) = n_0(1 + 0.01 \cdot (x - 0.5) + 0.001 \cdot \cos(2\pi y)), \tag{4.6}$$

we find the results plotted in Fig. 4.4(a). In this case clearly a plateau appears and a wide minimum in R_{xx} is visible. Inhomogeneities in the current density can also
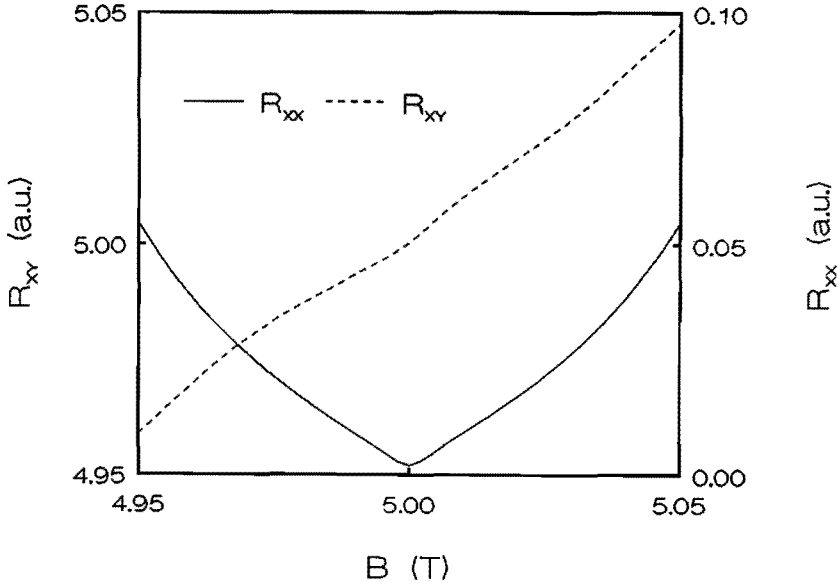
Fig. 4.3 *Calculated values of R_{xy} and R_{xx} determined from $V(0,17/70) - V(1,17/70)$ and $V(0,0) - V(0,1)$ respectively in case of a fixed electron distribution according to Eq. (4.5). Instead of a plateau only some structure is visible. The Shubnikov-de Haas minimum is rather sharp.*
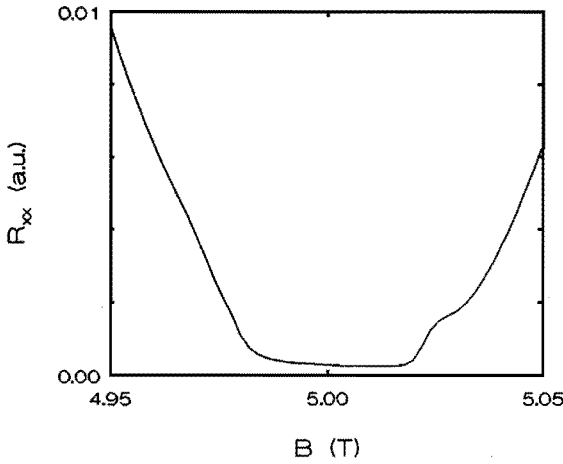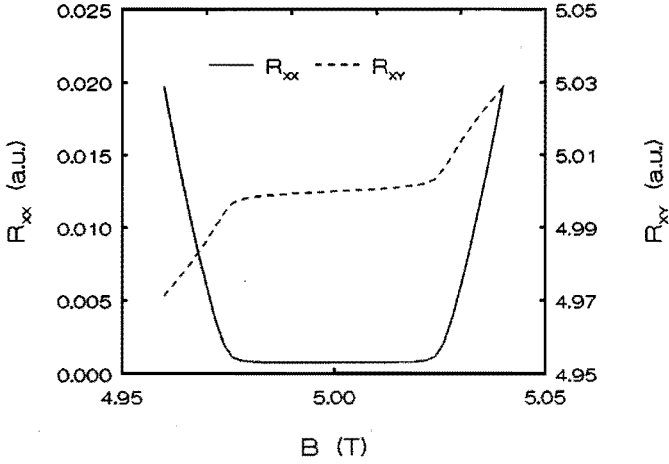
Fig. 4.4 *Calculated values of R_{xy} and R_{xx} determined from $V(0,0)-V(1,0)$ and $V(0,0)-V(0,1)$ respectively in case of a fixed electron distribution according to Eq. (4.6). A plateau and a wide R_{xx} minimum are visible (a). Calculated value of R_{xx} determined from $V(0,0)-V(0,1/5)$ in case of a fixed electron distribution according to Eq. (4.6). Clearly structure appears due to the inhomogeneous electron distribution (b).*

cause a structure to appear in R_{xx}, as will be clear from Fig. 4.4(b). Here, R_{xx} 'as measured' over a part of the structure is plotted.

The question arises why in these calculations a plateau shows up, whereas in the first choice of parameters (Eq. (4.5)) only some vague structure was visible. In both cases (Eqs. (4.5) and (4.6)) percolating paths are present which have constant ρ_{xy}. In addition, one of these paths, namely the one at integer filling factor, has a relatively low ρ_{xx}. Apparently, in order to obtain a plateau these current paths must exist over a broad range of magnetic fields. This condition is only fulfilled for the parameters chosen in Fig. 4.4 (Eq. (4.6)) and not for Fig. 4.3 (Eq. (4.5)).

From other calculations, which we do not show here, it became clear that the percolating ρ_{xy} paths are extremely 'wanted' by the current, especially when ρ_{xx} is much smaller than ρ_{xy}. This is caused by the effect, described at the beginning of this section, that boundaries between regions with different ρ_{xy} cause a strong deflection of the current path. The current is more or less obstructed by a change in ρ_{xy}. The effect is that strong that a percolating path of very low ρ_{xx} may be avoided if ρ_{xy} is not constant along this path. Instead a path with constant ρ_{xy} may be chosen, although ρ_{xx} is considerably higher. Without a magnetic field the path with low ρ_{xx} is favoured.

From the discussion mentioned above it is clear that the conditions necessary to observe a plateau are generally not fulfilled if we have to deal with a fixed random distribution of the electron density. This model of fixed inhomogeneous n does not give a correct explanation of the quantized Hall effect.

In Fig. 4.5 we plotted the current distribution in the case of $n(x,y)$ as defined in Eq. (4.5). The lines plotted are the trajectories along which the current flows. At $B = 5.0$ T the current runs predominantly along the edges of the sample. One can also see that the interior parts of the sample do not contribute much to the current and are more or less localized. This effect is stronger when ρ_{xx} is chosen such that it has a deeper minimum as a function of magnetic field. If we look at the current distribution at a different magnetic field value ($B = 4.9875$ T) we observe that the situation has completely changed. Now current flows also in the interior of the sample. This means that localized states have now become extended states. Therefore our picture of the localized and extended states differs from the 'normal' homogeneous localization picture with extended states in the centre of the Landau level and localized states in the wings of the Landau levels.

We now turn to the second model, in which we have a fixed potential landscape. In this case we perform the calculations as a function of the electron concentration (or ϵ_F). If calculations as a function of B are performed ϵ_F has to be determined self-consistently at every step in B in order to keep the total number of electrons fixed. We took for $D(\epsilon)$ semi-ellipses[12] with a width Γ. For $T = 0$, σ_{xx} was then calculated from $\sigma_{xx} = c \cdot D^2(\epsilon_F)$. The result of one of our calculations is shown in Fig. 4.6. Here we took

$$\epsilon = \epsilon_c \cdot \sin(\pi x) \cdot \sin(2\pi y), \tag{4.7}$$

with $\epsilon_c = 1$ meV, $\Gamma = 1$ meV and $\hbar\omega_c = 10$ meV; the Fermi level moves from the fourth to the fifth Landau level. It is clearly visible from Fig. 4.6. that a wide plateau appears. Also a wide minimum in R_{xx} is present. Thus, within this picture it is possible to achieve plateaus, although at zero magnetic field the situation is comparable to that of Eq. (4.5) where no plateaus appear (see Fig. 4.3). The reason for this behaviour is that the charge redistribution facilitates the occurrence of
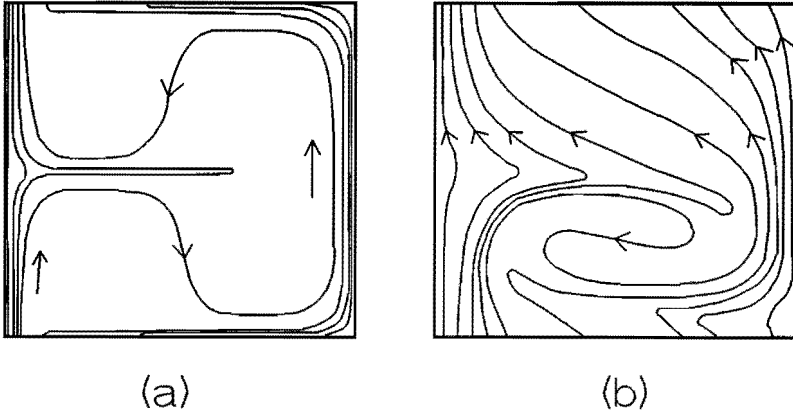

(a)   (b)

Fig. 4.5 *Current distribution at 5.0 T (a) and 4.9875 T (b). The electron distribution is given by Eq. (4.5). Drawn are the lines along which the current flows. Between every two adjacent lines an equal amount of current flows. It is clear that more or less localized regions exist, the position of which depends on the magnitude of B.*

percolating ρ_{xy} paths, or even entire areas, at integer filling factors. Since these charge redistribution effects almost certainly exist, the quantized Hall plateau width may be partially or completely due to this effect. The experimental observation that low mobility samples show wider plateaus than samples with a high mobility may imply that a low mobility is accompanied by a low homogeneity.

For two other cases we calculated the potential distribution, i.e. for

$$\epsilon = \epsilon_c \cdot (\ (1 + \cos(2\pi x)) \cdot (1 + \cos(2\pi y)) - 2\ ),$$
$$\epsilon' = -\epsilon, \tag{4.8}$$

both with $\epsilon_c = 0.175$ meV, $\Gamma = 1$ meV and $\hbar\omega_c = 10$ meV. The result is indicated in Fig. 4.7. We immediately see that an asymmetrical shape of the R_{xx} curve occurs. The asymmetry clearly depends on the shape of the ϵ-distribution and looks similar to the one measured by Haug et al[16]. Haug demonstrated experimentally that the
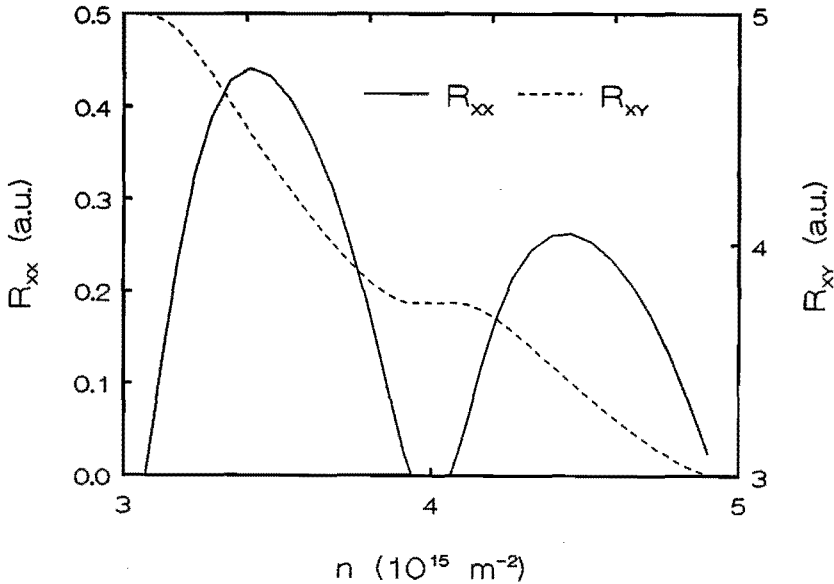

Fig. 4.6   *Calculated values of R_{xy} and R_{xx} determined from $V(0,7/12) - V(1,7/12)$ and $V(0,0) - V(0,1)$ respectively in case of a fixed ϵ-distribution according to Eq. (4.7). Clearly a plateau and a wide R_{xx} minimum occur.*

asymmetry depends on the type of scatterers present. He argued that these scatterers would modify the density of states in such a way that it would become asymmetrical. In our calculation it is not the density of states which is asymmetrical, but the ϵ distribution. This asymmetry could also be caused by the scatterers. At present we are not yet able to calculate the temperature dependence of the asymmetry. From experimental observations, however, we know that increasing the temperature decreases the asymmetry. We think this is because the inhomogeneity decreases with increasing temperature since a broad Fermi-Dirac distribution smooths the electron distribution. In addition a similar asymmetry observed in narrow samples[17] was interpreted in the same terms by assuming an inhomogeneity in ϵ caused by the edges.

The local current densities we calculated are all due to an externally imposed current. In the Büttiker model[7], however, there exists a local non-zero current density at the edges without any imposed external or total current. This is a
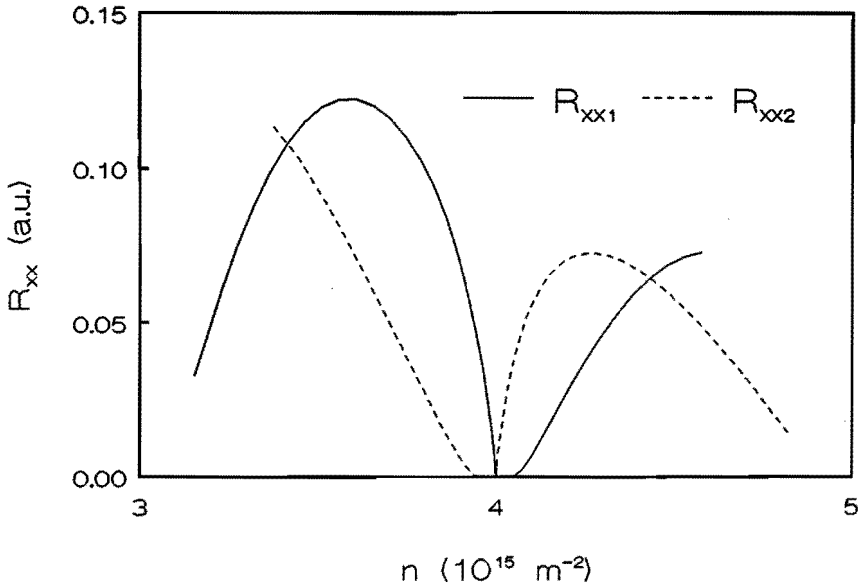

Fig. 4.7   *Calculated values of R_{xx} determined from $V(0,2/5) - V(0,3/5)$ in the case of a fixed ϵ-distribution according to Eq. (4.8) and in case of ϵ' with $\epsilon'=-\epsilon$. Clearly visible is the asymmetrical shape of the Shubnikov-de Haas oscillations.*

consequence of the band bending of the Landau levels at the edges, see Fig. 3.4 and the group velocity which obeys Eq. (3.6). A non-zero drift velocity can of course also be present due to internal electric fields. So a non-zero current density is not restricted to the geometrical edges of the sample.

Consider for example the situation of Fig. 4.8 where we assume an inhomogeneous electron concentration to be present with a surplus of electrons in the centre. The local electrostatic potential distribution shows equipotential lines like indicated in Fig. 4.8(a). Hence, in a magnetic field currents appear parallel to these equipotential lines even in the absence of an externally applied current. If we now add a homogeneous current density the resulting total current density looks like indicated in Fig. 4.8(c) and (d) and the result depends on the magnitude of the
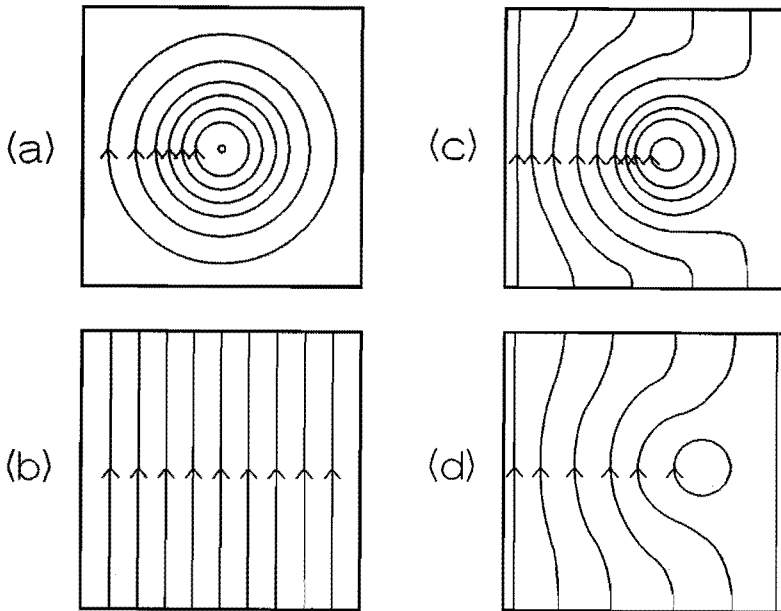

Fig. 4.8   *Electrostatic potential distribution, with its 'frozen in' current distribution (a). If an extra current distribution (b) is imposed the resulting total current distribution (c) and (d) depends on the magnitude of the imposed current distribution. The larger current is added in (d).*

current added. It is shown that although a homogeneous current density is added, the resulting total current density is highly inhomogeneous and that it becomes more homogeneous if a larger current is added. In the next chapter we will determine the current distribution due to these externally imposed currents.

In conclusion we state that a magnetic field can strongly influence the current distribution in the two-dimensional electron gas. The current flows preferably along equi-ρ_{xy} lines if ρ_{xx} is small compared to ρ_{xy}. Furthermore, if the quantized Hall effect is to be explained solely by inhomogeneities it is inevitable to assume charge redistribution in the sample when changing the magnetic field. Inhomogeneities can also cause structure in R_{xx} at the plateau edges and asymmetrical R_{xx} curves.

4.3 Which types of inhomogeneities are present and how to detect them

Within the scope of this thesis only those (spatial) inhomogeneities are of importance which show up in the electrical transport properties of the two-dimensional electron gas, like an inhomogeneous electron concentration or inhomogeneous mobility. Principally these are all caused by inhomogeneities in the composition or structure of the $GaAs/Al_xGa_{1-x}As$ heterostructure, which are determined during the growth.

Predominantly the distribution of Si-donors throughout the doped $Al_xGa_{1-x}As$ and the degree of perfection of the GaAs and $Al_xGa_{1-x}As$ layers are of importance. These do not only influence the scattering time, but especially the Si-distribution has its impact on the shape and depth of the potential well at the $GaAs/Al_xGa_{1-x}As$ interface and hence on the electron concentration. Thus a band bending can occur parallel to the interface due to electric fields parallel to the interface and spatial variations in the local electrostatic potential are present. It is clear that this also occurs at the edges of the heterostructure where the Si-doping level jumps to zero. This causes the electron concentration to decrease steeply at the edges. From electrical transport measurements on narrow heterostructures[18] ($< 1\ \mu$m) it can be deduced that these edge effects, which can be looked at as inhomogeneities, occur over distances of about 100 nm. Further, several types of defects like dislocation lines and oval defects have a severe impact.

The long range homogeneity of complete wafers can easily be investigated by cutting out small pieces and subsequent examination of their electrical properties. The result of such an experiment is of course some spatial average over the sample under study. This kind of measurement usually indicates a variation of the electron concentration and mobility less than a few percent over distances of about 1 cm.

Sometimes variations of the same order of magnitude can be observed over much smaller distances. These inhomogeneities manifest themselves in the difference between signals, measured across different pairs of contacts attached to one and the same Hall bar, which should behave equivalently. Care should be taken, however, when interpreting the experimental results. Short range variations are not necessarily an indication of an inhomogeneous electron concentration. As we will discuss later there might be local interruptions in the two-dimensional electron gas on an atomic scale. These consist of very narrow crack-like structures up to about 1 mm long which have a very high resistance. These cracks were first discovered by a liquid crystal technique[19]. If these interruptions are present the geometry of the structure is altered and the different pairs of contacts are no longer equivalent. Apart from the cracks also a really inhomogeneous electron gas might be present. This is not necessarily a consequence of an inhomogeneous Si-distribution, but it can be due to an inhomogeneous distribution of electrons over the dopant atoms. This kind of situation can occur at low temperatures, where such an instable situation can be frozen in. It is commonly known in this field of semiconductor physics that the homogeneity of the electron concentration, as observed in electrical transport experiments, strongly depends on the cooling-down procedure, i.e. slow or fast cooling with or without the presence of stress and/or light. This makes the comparison between measurements obtained during different cooling-down cycles difficult.

In addition to these electrical transport experiments also several (electro-) optical techniques are suited to characterize the two-dimensional electron gas. With these techniques one can in principle obtain a spatial resolution of the order of the wavelength of the light used or at least the diffusion length of the charge carriers.

Photoluminescence techniques on complete wafers[20] have revealed inhomogeneities comparable to those obtained by electrical transport measurements. But photoluminescence measurements can also be used to detect individual defects of about several μm. Small changes over small distances, however, are hard to measure.

A technique which is very well suited to image the quality of heterostructures quickly is the lateral photo effect[21,22]. In this kind of experiment electron-hole pairs are created in the GaAs by an incident spot of light and a normal photovoltage builds up between the two-dimensional electron gas and the p-side of the GaAs. Due to the local character of the illumination lateral (parallel to the surface) currents appear and a lateral photovoltage is established. This voltage can be measured across two contacts connected to the two-dimensional electron gas. It can be shown that in a homogeneous material the voltage depends linearly on the position of the illuminated spot between the contacts. Deviations from this linear dependence are an indication of inhomogeneities like dislocation lines. In this way the cracks we mentioned earlier in this section can be detected easily. It turns out that nearly all samples contain these cracks which we think to be dislocation lines, because they run parallel to the crystallographic axes. A surprising effect concerning these cracks is the fact that they seem to appear spontaneously after some storage time of e.g. one month. With a differential technique[23] we were able to image the local resistivity directly. In this way we are able to visualize defects with even higher resolution.

We mentioned in the introduction that electro-optic measurements are also suited to characterize GaAs[24]. This technique is based on the fact that GaAs becomes birefringent under an applied electric field. Light polarized along the fast and slow axes of the GaAs obtains a phase difference. See section 5.2 for an extensive discussion of this technique. With this method the spatially resolved potential distribution of the two-dimensional electron gas can be measured. Under quantized Hall conditions surprising results have been obtained, which we present in chapter 5.

The last technique we want to mention here is etching, with which all sorts of microscopic defects can be observed. The technique is based on the fact that defects usually have a higher etch rate. Though, this is a destructive technique and it does not reveal slight inhomogeneities over larger distances.

To conclude this section we state that inhomogeneities are always present. Every device should be checked for larger defects like dislocation lines by means of e.g. a scanning optical microscope (application of the lateral photo effect) prior to performing other electrical transport measurements. Although the presence of several inhomogeneities can be detected, there is insufficient information about

small inhomogeneities ($< 1\%$) or larger inhomogeneities over small distances ($< 1\,\mu$m), e.g. clusters of Si-atoms in the doped $Al_xGa_{1-x}As$. Unfortunately, as we have seen in section 4.2, the very small (unknown) inhomogeneities in electron concentration ($< 0.1\%$) can have a considerable influence on the current distribution in high magnetic fields.

CHAPTER 5

OPTICAL MEASUREMENT OF THE SPATIAL POTENTIAL DISTRIBUTION IN THE QUANTIZED HALL EFFECT

5.1 Why contactless measurements?

Until recently, experimental access to the problem of the current and potential distribution in two–dimensional electron gases under quantized Hall conditions was possible only by attaching electrical contacts[10,11] to the interior of the two-dimensional electron gas. These electrical contacts, however, disturb the system to be investigated. First, the contact acts as an equipotential probe; it is an electron reservoir with a thermalized electron distribution. Second, there are problems arising from the so–called Corbino effect. Finally, by attaching an electrical contact, the electrochemical potential rather than the electrostatic potential is measured. With these problems in mind it is not clear whether the effects of current bunching reported in Refs. 10 and 11, see Fig. 1.2, are due to the presence of the electrical contacts or due to an intrinsic effect in the two-dimensional electron gas.

Our technique to determine the spatial potential distribution is based on the linear electro–optic effect[25] or Pockels effect and makes use of the effect that GaAs becomes birefringent when an electric field is applied. The application of the Pockels effect is not uncommon in the field of GaAs chip testing[26], but has until recently never been applied under quantized Hall conditions. Since it is a technique which does not involve electrical contacts we avoid the problems mentioned above.

In section 5.2 we describe the experimental set-up and in section 5.3 we present our experimental results in combination with a discussion and a comparison with theoretical models.

5.2 Details of the experimental set-up

GaAs becomes birefringent when an electric field is applied. We can take advantage of this effect to determine the potential difference between the two-dimensional electron gas and the back–gate of a GaAs/Al$_x$Ga$_{1-x}$As heterostructure. This has been demonstrated in Ref. 24. We will briefly outline the method here.

We used a 1.3 μm, 1 mW semiconductor solid–state laser beam, which is focused, with a focal diameter of 70 μm, on a GaAs/Al$_x$Ga$_{1-x}$As heterostructure with a two-dimensional electron gas in the (001) plane, see Fig. 5.1. The light is polarized along the <100> axis and travels in the <001> direction. Since the GaAs is transparent to the wavelength of 1.3 μm, the light exits on the back of the substrate, on which we evaporated a thin (8 nm) semi–transparent Au–layer acting as an equipotential plane. When a potential difference V is present between the two-dimensional electron gas and the Au–layer, the components of the light polarized
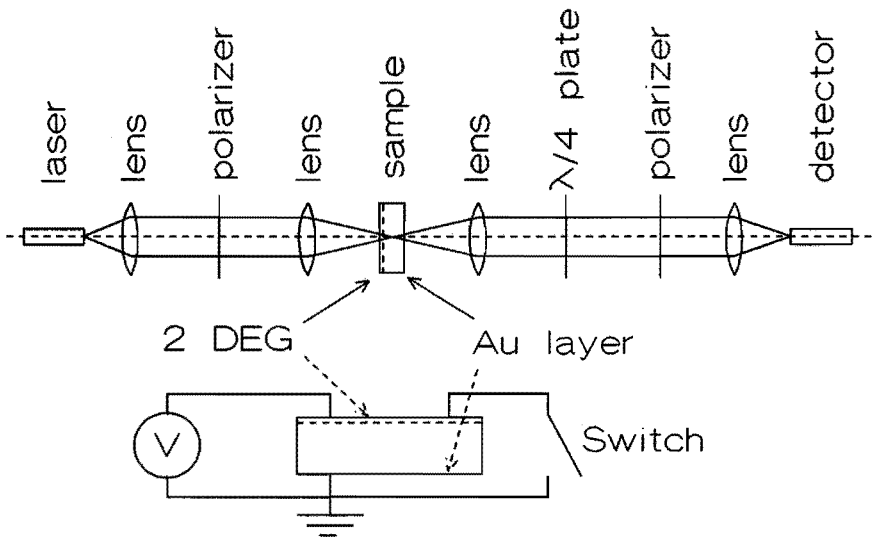

Fig. 5.1 *Experimental set-up, the electrical circuit is indicated schematically.*

along the fast and slow axes obtain a phase difference $\Delta\Gamma$. It has been shown[25,26] that this phase difference $\Delta\Gamma$ equals

$$\Delta\Gamma = 2\pi/\lambda \; n_0^3 \; r_{41} \int\limits_0^d E_z(x,y,z)\mathrm{d}z = 2\pi/\lambda \; n_0^3 \; r_{41} \; V(x,y), \qquad (5.1)$$

where n_0 and r_{41} are the refractive index and the component of the electro–optic tensor of the GaAs, d is the thickness of the substrate, E_z the component of the electric field perpendicular to the two-dimensional electron gas and λ the wavelength. The electric field parallel to the two-dimensional electron gas does not enter this expression. If we position a quarter-wave plate and a polarizer in front of the detector the transmitted light intensity varies almost linearly with the applied potential difference between the two-dimensional electron gas and the Au–layer.

Since we do not want the incident laser beam to ionize additional donors and thus disturb the potential distribution, we apply a constant background illumination which empties all donor states in the $Al_xGa_{1-x}As$. We carefully selected a $GaAs/Al_xGa_{1-x}As$ heterostructure to ensure that even under illumination there is no parallel conduction in the $Al_xGa_{1-x}As$ layer. This is essential, because parallel conduction might cause a potential drop in the $Al_xGa_{1-x}As$. Since the $Al_xGa_{1-x}As$ also shows the Pockels effect, additional unwanted phase shifts in the transmitted light might then occur. However, as long as the $Al_xGa_{1-x}As$ is insulating, the potential drop in the very thin $Al_xGa_{1-x}As$ layer is negligibly small.

Our sample consists of a 400 μm GaAs substrate with on one side the 8 nm Au–layer kept at ground potential. On the other side a 4 μm GaAs buffer layer, a 20 nm $Al_xGa_{1-x}As$ spacer layer, a 40 nm $Al_xGa_{1-x}As$ Si–doped ($n_{Si} = 2\cdot10^{24}$ m^{-3}) layer (both with $x = 0.3$) and a 18 nm GaAs cap layer are grown. The sample has a rectangular geometry of 5.4 mm length and 2 mm width without side arms. Current contacts (In) were alloyed into the two-dimensional electron gas at both ends, 5.4 mm apart. Prior to our experiments we checked the homogeneity of our sample with a laser–scan technique to be sure that no interruptions of the two-dimensional electron gas[21] or other major defects are present.

To avoid interference effects the sample is slightly tilted from normal incidence ($\approx 7^{\circ}$). Due to this tilt angle, electric fields parallel to the two-dimensional electron gas also enter Eq. (5.1). The impact of the error introduced by this tilting will be discussed later on in relation to the presence of fringing fields. As the potential differences to be detected are fairly small we apply an alternating current (235 Hz) through the two-dimensional electron gas and thus modulate the transmitted light intensity. The detector output is hence measured with a lock–in technique. We carefully checked that the measured signals had neither an out of phase component nor a double frequency component.

In order to determine the local potential in the two-dimensional electron gas we first perform a calibration measurement. To this end an alternating voltage of 5.6 V_{pp} is applied between the two-dimensional electron gas and the Au–layer, which is at ground potential, and the resulting detector signal is measured. Next, an alternating current of known amplitude is sent through the two-dimensional electron gas, with one current contact and the Au–layer at ground potential, and again the lock–in signal is measured. Both measurements are taken at the same position of the laser beam. The ratio of the detected intensities in these two measurements yields the unknown potential at the position of the laser beam for the case of the alternating current flowing through the two-dimensional electron gas. Subsequently the laser beam is scanned across the surface of the sample step by step. At each spot the calibration procedure is repeated. We checked that the results do not depend on the amplitude of the voltage applied in the calibration measurement. Further, the use of alternating currents with current reversal in the sample does not cause any problems, since our results are the same if we apply a DC offset current. With this DC offset current we obtain a modulated current density which is not reversed. Therefore we can rule out that spatial switching of current paths affects our measurements. As a last confirmation of the correctness of our experimental results we note that measurements performed during the same cool-down cycle reproduce very well.

5.3 The results and their interpretation in terms of edge charge

The result of a two-point resistance measurement as a function of magnetic field is shown in Fig. 5.2. Due to the two-point character of the method both Hall plateaus and Shubnikov-de Haas oscillations are visible. From Fig. 5.2 an electron concentration of $5.0 \cdot 10^{15}$ m^{-2} and a mobility of 20 m^2/Vs can be derived. In the following we subsequently present and discuss line scans of the potential made at the magnetic field values indicated in Fig. 5.2. Unless indicated otherwise the temperature at which these scans are made is 1.5 K.

The first two scans, see Fig. 5.3, are made inside the plateau with filling factor four. These are scans across the width of the Hall bar in the middle between the current contacts. The edges of the Hall bar are at ±1 mm. It is obvious from Fig. 5.3 that the Hall potential steeply increases or decreases at the edges. In the interior a more or less linear dependence on position is observed. If the temperature is

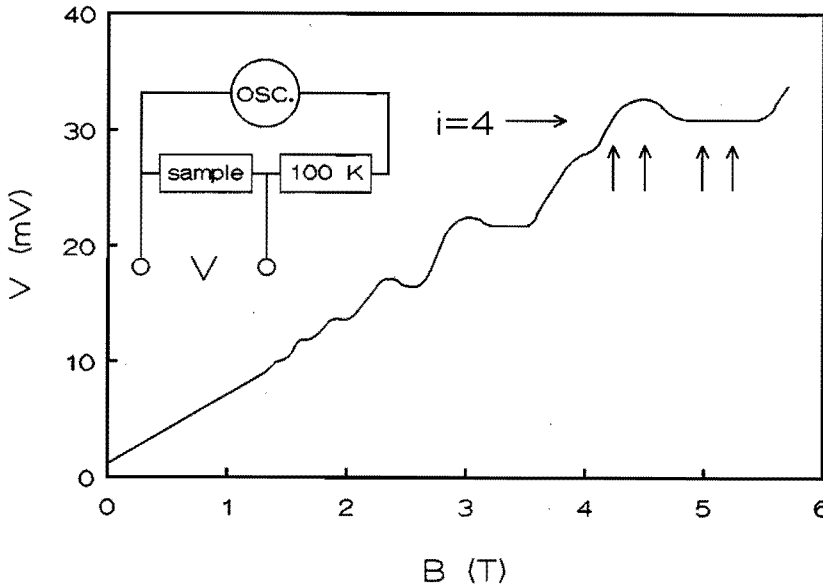**Fig. 5.2** *Plot of the voltage across the sample versus magnetic field (I = 5 µA, T = 1.5 K). The two-point experiment shows both plateaus and Shubnikov-de Haas oscillations. Arrows indicate magnetic field values at which line scans are made.*

raised to 55 K, see Fig. 5.4, the edge effects disappear and a linear dependence of the Hall potential on position is observed. The measured potential difference is equal to the Hall voltage measured electrically on the Hall probes. This observation implies that there are no disturbing fringing fields at the edges. Prior to the presentation of further measurements we now first turn to the theoretical interpretation of these results.

We have already mentioned at the end of section 4.2 that far away from the current contacts in a homogeneous sample also a homogeneous current distribution is expected to occur, irrespective of the magnitude of the magnetic field as long as $\sigma_{xx} \neq 0$. This can easily be derived from the substitution of Eq. (3.1) in Eq. (4.1), which leads to

$$\sigma_{xx} \left(\partial^2 V / \partial x^2 + \partial^2 V / \partial y^2 \right) = 0. \tag{5.2}$$

This can be compared with Eq. (4.4), which is the more general equation for the
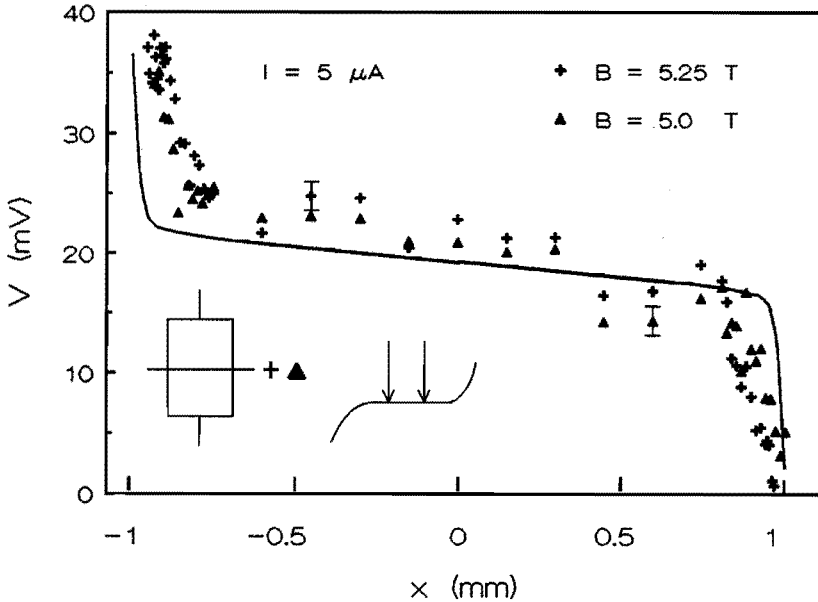
Fig. 5.3 *Two line scans of the potential at magnetic fields of 5.0 T (▲) and 5.25 T (+). The solid line is the result of a model calculation (Eq. (5.6)).*

inhomogeneous case. If we assume the current to flow in the y-direction and if we assume an infinitely long homogeneous sample, we can show that $\partial V/\partial y = $ constant, and hence $\partial^2 V/\partial y^2 = 0$. Thus it follows from Eq. (5.2) that in the homogeneous case also $\partial^2 V/\partial x^2 = 0$ (if $\sigma_{xx} \neq 0$) and hence $\partial V/\partial x = $ constant, which implies a homogeneous Hall field and hence a homogeneous current distribution. This is what we observe at 55 K (Fig. 5.4) where the quantized Hall effect is absent and hence $\sigma_{xx} \neq 0$.

If $\sigma_{xx} = 0$, however, this argument does not hold and the potential distribution has to be calculated by other means. This calculation has been carried out by MacDonald et al[27] and Thouless[28]. They argue that at integer filling factor a possibility exists to accommodate more charge per unit area in one Landau level. In an electric field all one electron wave functions (Eq. (3.7)) are shifted in space. If
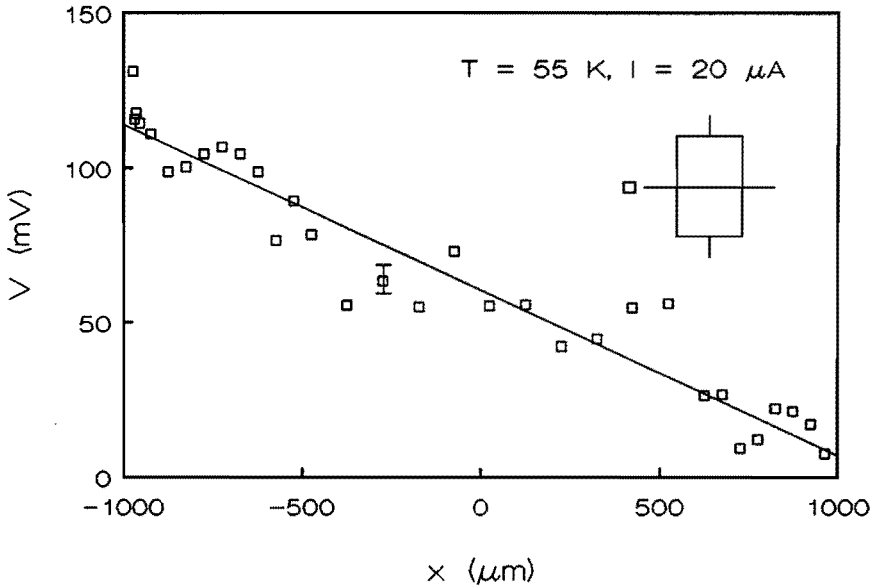
Fig. 5.4   *Line scan at 55 K, where the quantized Hall effect is absent. A linear potential distribution is observed (the straight line is a least squares fit).*

the electric field depends on position this shift and hence the electron density depends on position too, according to[27,28]:

$$n_{\text{excess}} = m^* i / \hbar B \; \mathrm{d}^2 V_{\text{H}}(x) / \mathrm{d}x^2, \qquad \text{for } -\tfrac{1}{2}W < x < \tfrac{1}{2}W, \tag{5.3}$$

with W the width of the sample. In this way it is possible to maintain an integer filling factor throughout the sample despite charge redistribution. The potential is related to the excess density by

$$V_{\text{H}}(x) = \frac{-e}{2\pi\kappa} \int_{-W/2}^{+W/2} n_{\text{excess}} \ln|x_1 - x| \; \mathrm{d}x_1, \tag{5.4}$$

with κ the dielectric constant. So we have to solve the equation

$$V_{\text{H}}(x) = -\xi \int_{-W/2}^{+W/2} \mathrm{d}^2 V_{\text{H}}(x_1) / \mathrm{d}x_1^2 \ln|x_1 - x| \; \mathrm{d}x_1, \tag{5.5}$$

with $\xi = i l^2 / \pi a^*$, l the magnetic length (Eq. (3.8)) and $a^* = 4\pi\kappa\hbar^2 / m^* e^2$ the effective Bohr radius. This can be done numerically. For the limit of small ξ Beenakker[29] has shown that the solution of Eq. (5.5) can be approximated accurately by:

$$V_{\text{H}}(x) = \tfrac{1}{2} I \rho_{xy} \left(\ln \frac{W}{\xi} \right)^{-1} \ln \left| \frac{x - W/2}{x + W/2} \right|, \qquad \text{for } |x| \leq W/2 - \xi. \tag{5.6}$$

In our case ξ is small ($\xi = 1.6 \cdot 10^{-8}$ m at $B = 5$ T and a relative dielectric constant of 13 for GaAs). The variation of $V_{\text{H}}(x)$ within a distance ξ from the edges can be neglected. Eq. (5.6) approximates the potential as a result of line charge with width ξ at the two edges $x = \pm W/2$ of the Hall bar. In Fig. 5.3 we have plotted the potential distribution calculated from Eq. (5.6). The agreement with the experiment is striking in view of the fact that the theory does not contain any adjustable parameters.

Results of scans outside the plateau region are presented in Figs. 5.5(a) and (b). The almost linear increase of the Hall potential in the interior of the Hall
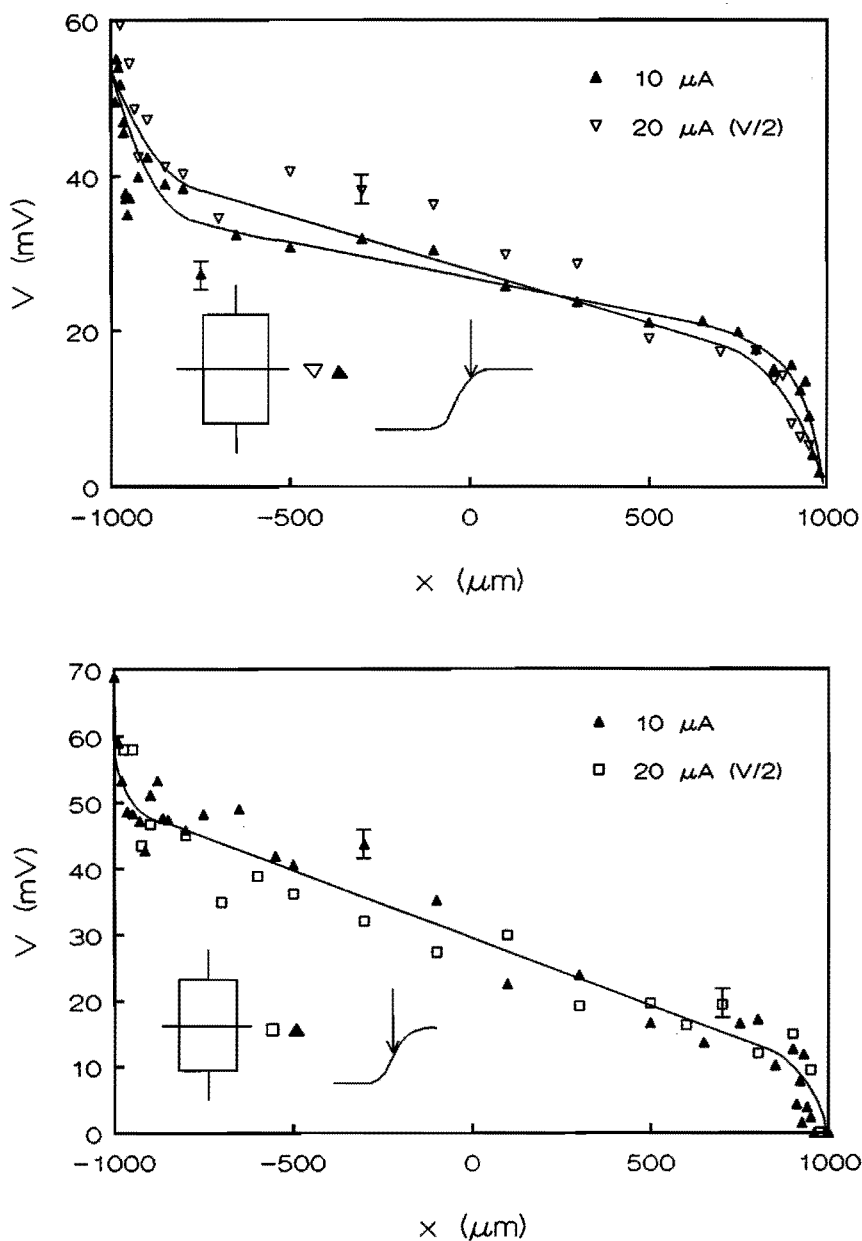
Fig. 5.5 *Line scans at a magnetic field of 4.55 T (a) (top) and 4.25 T (b) (bottom), both at 10 µA and 20 µA. Although the edge effects are smaller than inside the plateau region they remain present (lines are meant as a guide to the eye).*

bar becomes more pronounced the further the plateau region is left. Also outside the plateau the edge effects, although smaller, remain present. A similar transition to a linear potential distribution can be observed inside a plateau region if the current is increased, see Fig. 5.6. This can be explained by heating effects which cause ρ_{xx} to increase. If the current is increased far enough a linear behaviour (not shown), like that of Fig. 5.4, occurs.

These heating effects might be related to the large amount of electrons which pile up at the edges and the associated high electric fields. From Eq. (5.6) we deduce that at a distance ξ from the edge (with $i = 4$, $V_H = 0.1$ V), the Hall electric field equals $E_x = 3 \cdot 10^5$ V/m. This corresponds to a potential drop of 3 mV within a distance of 10 nm, which results in a substantial overlap of wave functions of adjacent Landau levels. Hence inelastic scattering processes may occur.
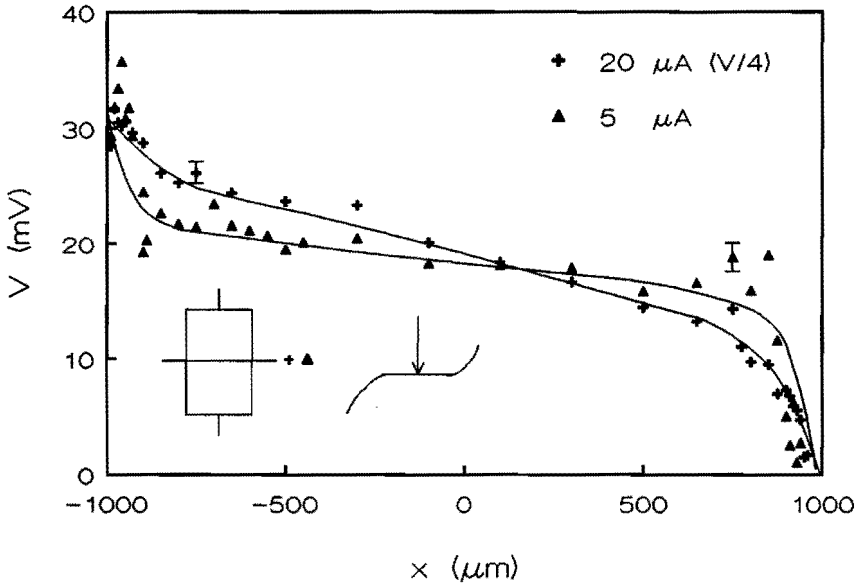

Fig. 5.6 *Line scans at 5 µA and 20 µA, in the centre of a plateau. A clear current dependence can be observed (lines are a guide to the eye).*

In between plateaus these high electric fields do not occur. The linear potential distribution which should develop if $\sigma_{xx} = \text{constant} \neq 0$ is associated by an excess electron concentration of[28]:

$$n_{\text{excess}} = 2\kappa V_{\text{H}}/eW \quad x/(\tfrac{1}{4}W^2 - x^2)^{1/2} \tag{5.7}$$

At a distance ξ from the edge and at $V_{\text{H}} = 0.1$ V, $B = 5$ T this results in $n_{\text{excess}} = 1.4 \cdot 10^{13}$ m^{-2}, which seems to be small regarding the magnitude of $n = 5.0 \cdot 10^{15}$ m^{-2}. However, since σ_{xx} can depend strongly on n, the condition $\sigma_{xx} = \text{constant}$ will no longer be fulfilled, even for such a small deviation from a homogeneous electron distribution. It is easy to see qualitatively what happens. Due to the translational symmetry of the problem the current flows parallel to the edges. The electric field E_y along this current is independent of position. Thus, since $E_y = \rho_{xx}J_y - \rho_{xy}J_x$ and $J_x = 0$, J_y is inversely proportional to ρ_{xx} everywhere. The Hall field as determined from the current distribution by $E_x = \rho_{xy}J_y$ is inversely proportional to ρ_{xx}. The magnitude of ρ_{xx} is determined by the distribution of the electrons over the density of states.

It is tempting to interpret the presence of edge effects in between the plateaus in terms of the above mentioned inhomogeneities induced by a large current. However, there are two major objections to such an interpretation. First, there should be a clear current dependence outside the plateau region as Eq. (5.7) depends on V_{H}. This, however, is not what we observe, although this may be due to our limited range of currents used. Second, the potential distribution should be asymmetrical due to an electron excess at one edge and a shortage at the other edge. This is not the case in Fig. 5.5.

Perhaps the clue to the presence of edge effects in between the plateaus can be found in the correspondence between the transition from inside to outside a plateau and the transition from low to high current inside a plateau. Both transitions are gradual. This resemblance might indicate that the underlying physics of both transitions is similar. If we assume that the sample is inhomogeneous, it is possible that the quantized Hall effect breaks down locally if the current is increased. In an inhomogeneous sample even outside a plateau the quantized Hall conditions may still be fulfilled in part of the sample. In this case the transition from the situation in Fig. 5.3 to Fig. 5.4 is no longer abrupt.

We now turn to the influence of electrical contacts. In Fig. 5.7 line scans along the length of the sample are presented. These scans are carried out at a current of 50 µA. At this large current the sample is heated up to some extent, but the measuring time is considerably reduced. The influence of the ends of the Hall bar with the current contacts is clearly visible. Fig. 5.7 shows that the current enters at one corner of the sample and exits at the opposite corner, as expected theoretically.

The influence of internal electrical contacts is much less clear. In Fig. 5.8 a scan across such an internal electrical contact is shown. We also show a scan 1 mm below the internal contact. The contact is disconnected. Note, however, that the measurement is not changed when we connect the contact to a lock-in amplifier with an input impedance of 100 MΩ to ground potential. Apart from the edge effects at the boundary of the two-dimensional electron gas we see a sharp bending of the measured potential in the immediate neighbourhood of the contact. The interpretation of this effect is yet unclear.
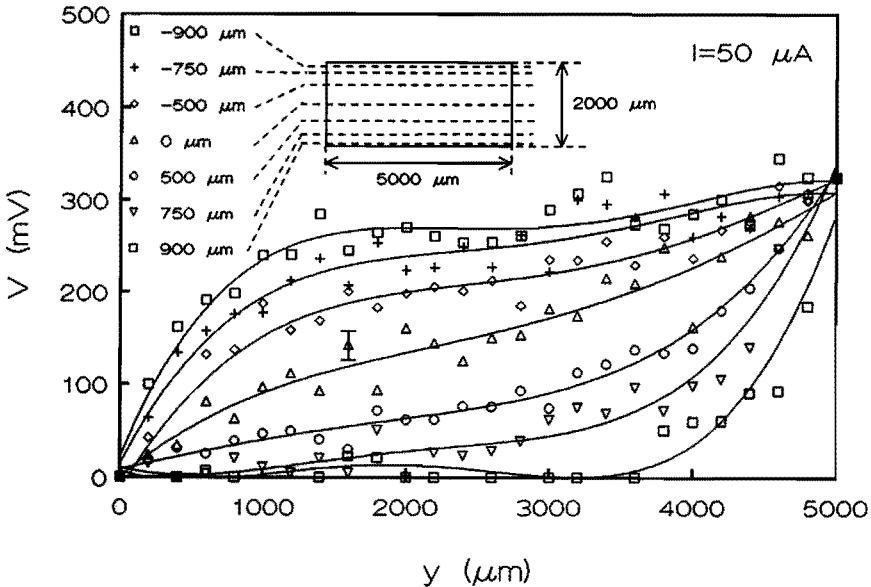

Fig. 5.7 *Line scans across the length of the sample at a current of 50 µA. The lines drawn are a rather arbitrary fit with polynomials of order four.*

We also measured the electrical potential between the interior electrical contacts and ground by attaching a voltmeter to the contact. The result is shown in Fig. 5.9. It is clearly different from Fig. 5.3. From Fig. 5.9 a current distribution would be obtained which strongly depends on the magnitude of the magnetic field. No such current distribution can be deduced from the Pockels experiment. This difference between the two experiments can be understood if one realizes that with electrical contacts one measures the electrochemical potential (the Fermi level), and that with the Pockels effect one measures the electrostatic potential. Already in a simple *pn*-junction, where the Fermi level is equal throughout the junction but the space charge at the interface of the junction causes an internal electric field, the electrochemical and electrostatic potential are different. One should be able to observe the resulting potential difference across such a junction with the Pockels effect, though not with a voltmeter.
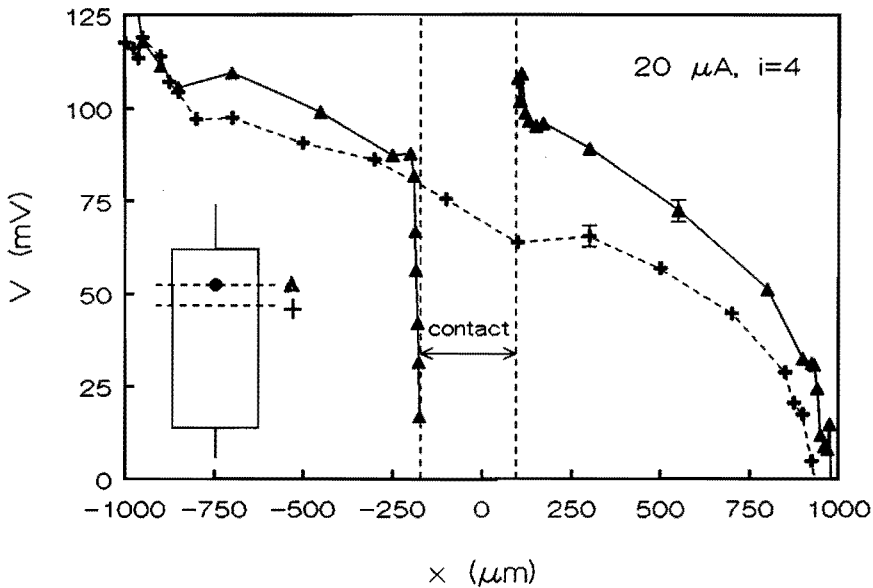

Fig. 5.8 *Line scan across and below an interior electrical contact. The lines are a connection of the data points.*

We now briefly reconsider the models of the quantized Hall effect which we discussed in sections 3.3 to 3.6. First we state that under our experimental conditions the entire Hall voltage across the Hall contacts is caused by an electrostatic potential difference. In the Büttiker model the driving force is diffusion due to gradients in the electron concentration. However, as pointed out earlier, see section 3.6 and Fig. 3.5, electric fields can be incorporated into the Büttiker model easily. The electrons simply obtain an extra drift velocity due to the electric field. If this incorporation is carried out and one assumes the electric field to be the entire cause of the Hall potential, then all ingredients of the Büttiker model which are essential to obtain the quantized Hall effect are simply those of Woltjer and Luryi, section 3.5. The essential assumptions made in these two models are a quantized Hall resistivity at integer filling factor in combination with long range ($\gg l$) inhomogeneities. This last requirement is imposed because a local resistivity must be definable within these models. However, we may also incorporate short range
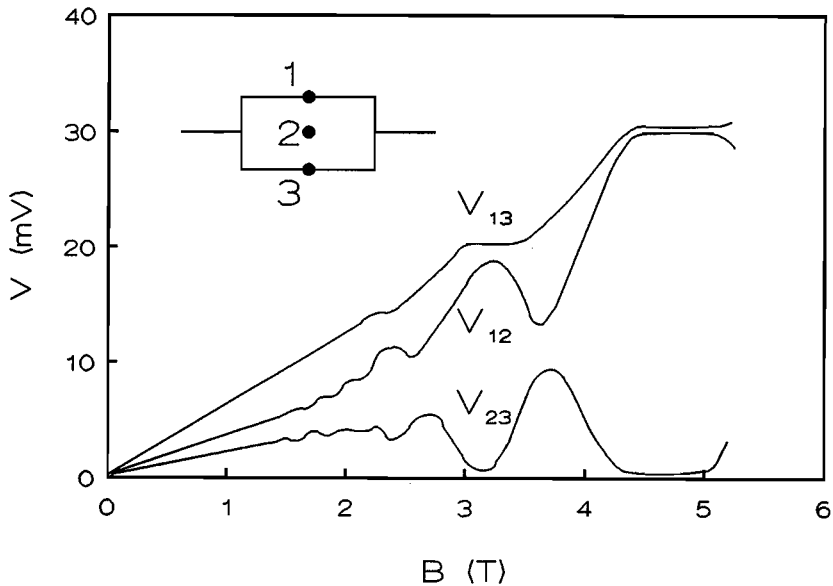
Fig. 5.9 *Hall potential measurement as a function of magnetic field between the contacts indicated. Contrary to the Pockels experiment, the current distribution seems to depend strongly on the magnetic field.*

inhomogeneities if we apply the arguments of Prange and Hansen, section 3.5, or Halperin and Laughlin, section 3.4. The short range inhomogeneities do not disturb the exact quantization at integer filling factor. If there are long-range inhomogeneities, then in between the plateaus the potential distribution is not completely linear, whereas in a plateau the potential distribution at the edges is not as steep as expected theoretically (Eq. (5.6)).

We conclude from our experiments that the Hall potential distribution in a plateau region is well described by the presence of edge charge. In between plateaus and at high current levels the Hall potential distribution becomes a linear function of position, with a gradual, sometimes incomplete change between both kinds of distributions. This indicates the coexistence of both regions with $\sigma_{xx} = 0$ and regions with $\sigma_{xx} \neq 0$ under these circumstances.

CHAPTER 6

THE QUANTIZED HALL EFFECT IN THE ABSENCE OF SAMPLE EDGES

6.1 The Corbino disc, a geometry without edges

The absence of edges which connect the two current contacts in a Corbino disc is its major difference with the Hall bar geometry. Because of this absence of edges a measurement of ρ_{xy} or σ_{xy} on such a structure would be a powerful tool to investigate the influence of the presence of edges on the quantized Hall effect. With the conventional magneto-transport techniques, however, such a measurement is an impossibility. The inability to do so is due to the fact that no tangential electric field can be developed in the Corbino disc. We circumvented this problem by modifying a technique of Syphers et al[30,31] who induce an electric field in the sample by application of a modulated magnetic field. The difference between their experiment and ours is that we load the Corbino disc with a resistor which is small compared to the resistance of the Corbino disc, instead of measuring an open-circuit voltage.

6.2 How to measure the Hall conductivity on a Corbino disc

We describe the modulated magnetic field which is applied perpendicular to the two-dimensional electron gas by

$$B(t) = B_0 + B_1 \sin(\omega t). \qquad (6.1)$$

The two contacts, see Fig. 2.2, are loaded with an impedance Z. The modulated magnetic field induces an electric field in the sample, which in turn causes a current to flow in the sample and in the impedance Z. We assume throughout the following

that the sample under study is homogeneous. In this case we can write down the following relation between the current density and the electric field:

$$E_\phi = \rho_{\phi\phi}J_\phi + \rho_{\phi r}J_r = \tfrac{1}{2}rdB/dt,$$
$$E_r = -\rho_{\phi r}J_\phi + \rho_{\phi\phi}J_r. \tag{6.2}$$

The indices r and ϕ indicate the radial and tangential components respectively. We can identify $\rho_{\phi\phi}$ with ρ_{xx} and $\rho_{\phi r}$ with ρ_{xy}. If the tangential current density is eliminated the radial electric field can be rewritten as

$$E_r = J_r(\rho_{xx}^2 + \rho_{xy}^2)/\rho_{xx} - \tfrac{1}{2}(\rho_{xy}/\rho_{xx})rdB/dt. \tag{6.3}$$

If we integrate Eq. (6.3) from the inner radius r_i to the outer radius r_o and use the relation $J_r = I/2\pi r$, with I the current through Z, we obtain

$$V = \frac{(\rho_{xy}/\rho_{xx})\tfrac{1}{4}(r_0^2 - r_i^2)dB/dt}{1 + \ln(r_o/r_i)/(2\pi Z\sigma_{xx})}. \tag{6.4}$$

In case $Z = \infty$ is substituted into Eq. (6.4) we get the relation derived by Syphers et al[30,31] with their geometry factor $f(r) = \tfrac{1}{4}(r_0^2 - r_i^2)$ and $\omega_c\tau = \rho_{xy}/\rho_{xx}$. The special limit we are interested in is obtained if $Z \ll Z_c$, with Z_c the resistance of the Corbino disc, $Z_c = 1/(2\pi\sigma_{xx})\ln(r_o/r_i)$. We can derive from Eq. (6.4) that in this limit

$$I = \tfrac{1}{2}\pi\sigma_{xy}(r_0^2 - r_i^2)/\ln(r_o/r_i)dB/dt. \tag{6.5}$$

With this expression we can determine σ_{xy} if we measure the current through the circuit.

A second possibility to determine σ_{xy} or ρ_{xy} on a Corbino disc, which is in fact very similar to the one described above, necessitates two separate measurements. The first experiment is just the one of Syphers (with $Z = \infty$) and yields ρ_{xy}/ρ_{xx}. The second experiment consists of a conventional measurement of the Corbino resistance and in this case $1/\sigma_{xx}$ is determined. From the ratio of these two quantities σ_{xy} can also be obtained (as $(\rho_{xy}/\rho_{xx})\sigma_{xx}) = \sigma_{xy}$).

6.3 The experimental absence of plateaus and its interpretation

The first experimental attempts to measure σ_{xy} made obvious that three major disturbing factors are present which cause signals which are orders of magnitude larger than those to be measured according to Eq. (6.5). These three are: vibrations of the wiring, thermo-voltages and a non-zero self inductance of the wiring.

Vibrations of the wiring in the static magnetic field result in large in and out of phase signals. Usage of one coaxial cable instead of two separate wires and careful fixation and positioning of this cable turned out to suppress this kind of inductive pick-up sufficiently.

The non-zero self inductance of the wiring, however, is harder to prevent. This self inductance is caused by small loops in the wires which connect the coaxial cable with the sample. Although it is relatively easy to trim this self inductance to zero at room temperature by means of an adjustable compensation coil, the self inductance appears again at low temperature due to thermal shrinking effects during cool-down. It was necessary to construct a compensation coil which is adjustable at liquid He temperature. One adjustable loop of about 1 mm^2 turned out to be sufficient.

Thermoelectric effects are the third disturbing influence we mentioned. Due to thermovoltages a DC current may appear in the circuit. As the resistance of the Corbino disc strongly depends on magnetic field in a plateau region the modulated magnetic field will modulate the Corbino resistance and hence this DC current too. This effect can be eliminated by inclusion of a capacitor in series with the load resistor, as it prevents DC currents. The value of this capacitor must be chosen such that its impedance can be neglected with respect to the resistance of the load resistor, in order to prevent both phase shifts and violation of the condition $Z \ll Z_c$.

For our σ_{xy} experiments presented below we use a modulation frequency of 2011 Hz, a 130 Ω resistor in series with a 47 μF capacitor and a modulation amplitude of 0.4 mT. The dimensions of the sample under study are $r_i = 200$ μm and $r_0 = 700$ μm ($n = 4.2 \cdot 10^{15}$ m^{-2}, $\mu = 15$ m^2/Vs at 2 K). With four Landau levels populated it can be calculated that this results in a current level of about 400 pA and a voltage of 55 nV across the resistor.

With the above mentioned precautions we obtained the experimental result plotted in Fig. 6.1. It is clear that the overall shape of the measured σ_{xy} curve corresponds to the expected $1/B$ behaviour. However, instead of plateaus we observe oscillations. 'Real' oscillations in σ_{xy} should only occur if ρ_{xx} is still sufficiently large. This because σ_{xy} is a mixture of ρ_{xy} and ρ_{xx} ($\sigma_{xy} = -\rho_{xy}/(\rho_{xx}^2 + \rho_{xx}^2)$). We checked that in our case the contribution of ρ_{xx} can be neglected and so this is not the origin of the oscillations in Fig. 6.1.

To check our set-up we also performed the second method we mentioned to determine σ_{xy}. Both the results of the normal Corbino measurement and the modulation method at high load impedance are plotted in Fig. 6.2(a). The ratio of these two, which should yield σ_{xy}, and the result of the direct determination of σ_{xy} (Fig. 6.1) are both shown in Fig. 6.2(b). As can be seen the results of the two methods look very similar apart from the somewhat larger noise in the full curve.
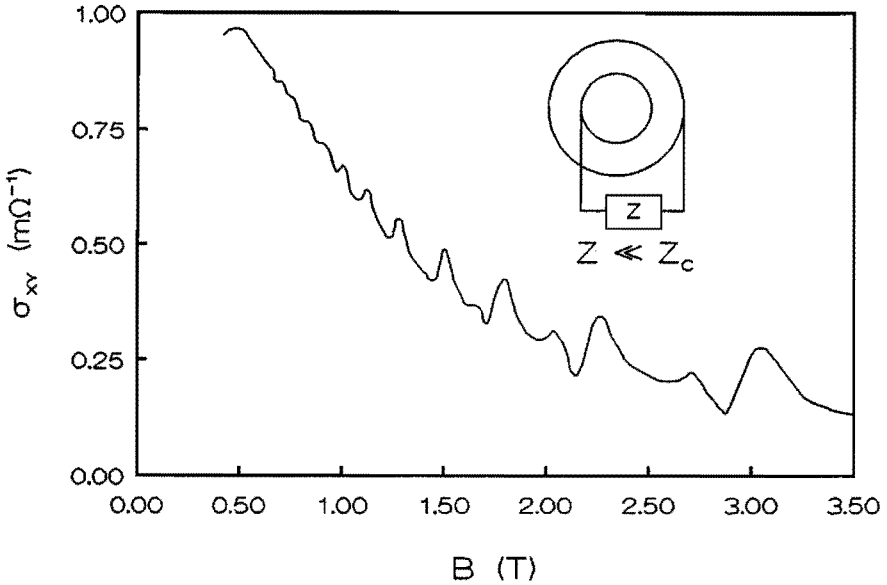
Fig. 6.1 *Hall conductivity σ_{xy} as a function of the magnetic field. A modulation frequency of 2011 Hz, a resistor of 130 Ω and a modulation of 5 Ts^{-1} are applied.*

Fig. 6.2 *Corbino resistance Z_c measured with an AC current of 6.4 nA (broken curve) and the induced voltage V_{ind} with $Z = 100$ MΩ (full curve) as a function of the magnetic field (a) (top). Hall conductivity σ_{xy} as calculated from Fig. 6.2(a) (full curve) compared with the measured conductivity (broken curve) (b) (bottom).*

These results are shown up to 2 T only because of the drastic increase of the Corbino resistance at higher fields, which becomes comparable to the input resistance of the measuring equipment.

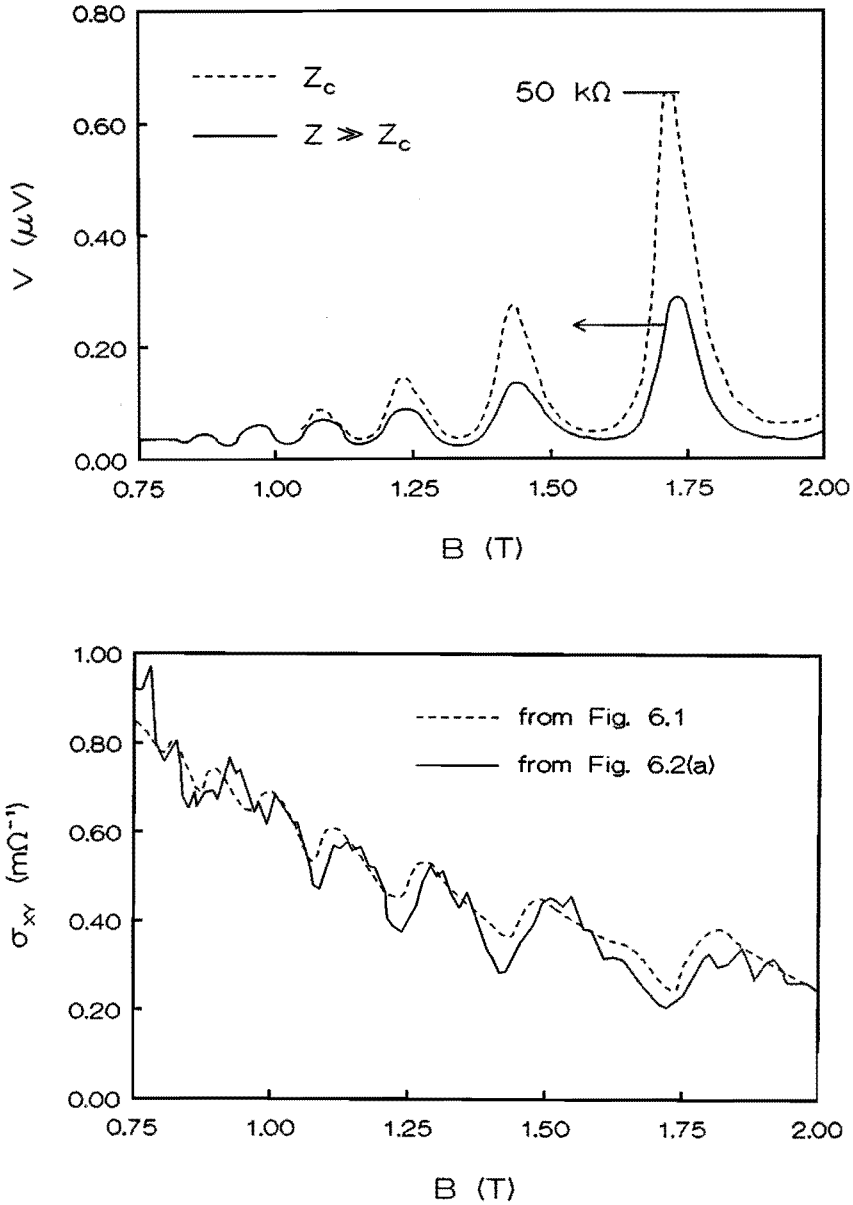At this point we wish to make some remarks on the accuracy of the method. From the modulation experiment with $Z = \infty$ the ratio ρ_{xy}/ρ_{xx} is obtained. Since we know the electron concentration we can identify the filling factor of the different plateaus and hence we know the corresponding values of ρ_{xy}. So we can calculate ρ_{xx} from this value and the measured ratio ρ_{xy}/ρ_{xx}. The values obtained agree within a few percent with the values calculated from the conventional Corbino measurement at the peak positions in Fig. 6.2(a). Furthermore we varied a number of experimental parameters. The applied frequency, load resistor, series capacitor and the magnitude of the magnetic field modulation had no significant influence on the shape of the oscillations as long as we stayed within reasonable limits. Increasing the temperature from 2 K to 10 K makes the oscillations disappear, but in this case the quantized Hall effect is expected to disappear as well. The exact shape and magnitude of the oscillations does depend, however, on the specific sample under study and the cool-down cycle. Cool-down dependent behaviour has already been mentioned in chapter 4, where we discussed sample inhomogeneities. So this experimental result may be an indication that the observed effects are indeed caused by sample inhomogeneities. To investigate whether this is the case we performed some model calculations we describe below.

For reasons of simplicity we chose in our calculations for a radial inhomogeneity in the electron concentration. Such an inhomogeneity seems rather arbitrary and artificial but might be caused during the processing of the sample, like for instance the fabrication of the electrical contacts. We took two concentrical areas with a difference in electron concentration of 0.4 % in a sample with the same dimensions as the one investigated experimentally. The boundary of these regions was taken to be situated at a radius of 450 μm. The values of ρ_{xy} are taken equal and constant in both areas. For ρ_{xx} a quadratic dependence on magnetic field is assumed and the position of the minimum value depends on electron concentration. To get the voltage across the sample we have to integrate Eq. (6.3) over the two parts and add them together. The resulting calculated signal, see Fig. 6.3, looks very similar to the experimentally observed ones, but the exact shape of the oscillation depends, of course, on the parameters used in the model calculation. Calculations with more

than two areas having different electron concentrations made clear that it is possible to model different shapes of oscillations. This also accounts for the cool-down dependence.

It is interesting to return to the question of the current distribution at this point. It might seem that the current is just radially directed in the homogeneous situation, this because the induced field is directed tangentially and the current flows at right angles to the electric field. Though, if we integrate along E_ϕ once around the Corbino disc we obtain a potential difference which depends on r as $\pi r^2 dB/dt$. Since this is not a constant, but depends strongly on r, there is no solution with radial currents only. The current must contain large tangential components. It can be derived from Eq. (6.2) that the current circulates clockwise around the centre contact and that this rotation becomes less strong with increasing r. At a specific radius there is no tangential component of the current and from that

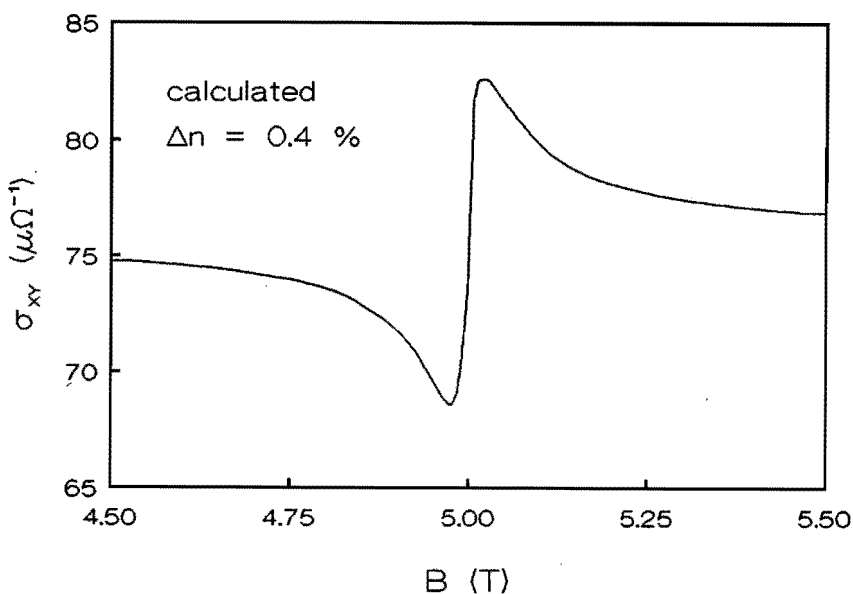

Fig. 6.3 *Calculated Hall conductivity σ_{xy} as a function of the magnetic field around a filling factor two. The difference in the electron concentration between the inner and outer part of the sample is 0.4 % in this calculation.*

point outwards the current flows counter-clockwise. When the sample is inhomogeneous this current distribution is even more complicated, like we discussed in chapter 4.

If we compare our experiments with the thought experiment of Laughlin (see chapter 3) we observe, apart from a striking similarity, the following difference. In our experiment the modulated field is present across the entire sample, in Laughlin's thought experiment the modulated magnetic field is restricted to the hole in the Corbino disc, or the inner contact, and Eq (6.5) becomes simply $I = \sigma_{xy} d\Phi/dt$. As a consequence a current distribution is possible with radial currents only in Laughlin's case. But this only in the special case that $\int \rho_{xx}/2\pi r \, dr = Z$ (integrated from r_i to r_o) and this can never be accomplished over a range of magnetic field values. Thus, in this case we will neither be able to observe plateaus if the sample is inhomogeneous.

In conclusion we can state that the method described does not deliver the expected Hall conductivity, but a conductance that strongly depends on inhomogeneities in the electron density. Such inhomogeneities do not disturb the quantized Hall plateaus in a Hall bar because of the different topology of the Hall bar. The results described give experimental evidence for the existence and the importance of inhomogeneities.

SUMMARY

This thesis deals with the investigation of the current distribution under quantized Hall conditions in two-dimensional electron gases present in $GaAs/Al_xGa_{1-x}As$ heterostructures. After a short introduction in chapter 1 to the contents of this thesis and in chapter 2 to the concept of the two-dimensional electron gas, we discuss in chapter 3 experiments and various models with respect to the quantized Hall effect. In chapters 4, 5 and 6 we present the results of our own investigations.

First, in chapter 4 the determination and calculation of the current distribution in inhomogeneous two-dimensional electron systems is presented. It is argued there that inhomogeneities can strongly influence the current distribution in high magnetic fields. We show that this can lead to specific structure in the Shubnikov-de Haas minima and to asymmetrical Shubnikov-de Haas peaks. Furthermore, the occurrence of quantized Hall plateaus is calculated for different types of sample inhomogeneities.

Second, in chapter 5 we present spatially resolved measurements of the potential distribution. These measurements are performed with an optical technique, which avoids the use of disturbing electrical contacts. Our results show that the potential distribution under quantized Hall conditions is determined by edge charge, which results in steep changes of the Hall potential at the edges. These steep changes disappear if the current or temperature is increased and if one leaves the plateau region.

Third, in chapter 6 the influence of the presence of sample edges on the occurrence of the quantized Hall effect is investigated. These investigations are carried out on a Corbino disc subjected to a modulated magnetic field. With this method the Hall conductance of the Corbino disc is determined. We find that the presence of inhomogeneities causes the plateaus to disappear, in contrast to what one observes in Hall bar structures.

SAMENVATTING

Dit proefschrift handelt over onderzoek aan de stroomverdeling in tweedimensionale electronengassen in $GaAs/Al_xGa_{1-x}As$ heterostructuren onder quantum Hall condities. Na een korte inleiding in hoofdstuk 1 over de inhoud van dit proefschrift en in hoofdstuk 2 over het concept van het tweedimensionale electronengas, beschouwen we in hoofdstuk 3 experimenten en enkele modellen betreffende het quantum Hall effect. In de hoofdstukken 4, 5 and 6 worden de resultaten van ons eigen onderzoek behandeld.

In hoofdstuk 4 worden berekeningen van de stroomverdeling in inhomogene tweedimensionale electronengassen gepresenteerd. Aangetoond wordt dat in hoge magneetvelden de inhomogeniteiten een grote invloed kunnen uitoefenen op de stroomverdeling. We laten zien dat dit kan leiden tot specifieke structuur in de Shubnikov-de Haas minima en tot asymmetrische Shubnikov-de Haas pieken. Voorts wordt het al dan niet optreden van het quantum Hall effect berekend voor verschillende inhomogeniteiten in het tweedimensionale electronengas.

In hoofdstuk 5 worden metingen getoond van de lokale potentiaal in het tweedimensionale electronengas. Deze metingen zijn uitgevoerd met behulp van een optische techniek waarbij storende invloeden van electrische contacten worden vermeden. Onze resultaten laten zien dat de potentiaalverdeling onder quantum Hall condities veroorzaakt wordt door lading aan de randen van de structuur, hetgeen aanleiding geeft tot een sterke plaatsafhankelijkheid van de potentiaal aan deze randen. Deze sterke plaatsafhankelijkheid verdwijnt als de stroom of temperatuur wordt verhoogd en als men het plateau verlaat.

In hoofdstuk 6 wordt de invloed van de aanwezigheid van preparaatranden op het optreden van het quantum Hall effect onderzocht. Dit onderzoek is uitgevoerd aan een Corbino schijf die geplaatst is in een gemoduleerd magneetveld. Met deze techniek is de Hallgeleiding van de Corbino schijf bepaald. Wij vinden dat de aanwezigheid van inhomogeniteiten de Hall plateaus doet verdwijnen, in tegenstelling tot hetgeen in Hall bar structuren wordt waargenomen.

REFERENCES

[1] for reviews see e.g. D.R. Yennie, Rev. Mod. Phys. **59**, 781 (1987), or "The Quantum Hall Effect", R.E. Prange and S.M. Girvin editors, Springer Verlag (1987). An elementary introduction to the quantum Hall effect has been written by B.I. Halperin in Scientific American (April 1986), 52.

[2] K. von Klitzing, G. Dorda, and M. Pepper, Phys. Rev. Lett. **45**, 494 (1980).

[3] R.F. Kazarinov and S. Luryi, Phys. Rev. B **25**, 7626 (1982).

[4] R. Woltjer, R. Eppenga, J. Mooren, C.E. Timmering and J.-P. André, Europhys. Lett. **2**, 149 (1986).

[5] R.E. Prange, Phys. Rev. B **23**, 4802 (1981).

[6] E.B. Hansen, Physica **123B**, 183 (1984).

[7] M. Büttiker, Phys. Rev. B **38**, 9375 (1988).

[8] R.B. Laughlin, Phys. Rev. B **23**, 5632 (1981).

[9] B.I. Halperin, Phys. Rev. B **25**, 2185 (1982).

[10] G. Ebert, K. von Klitzing, and G. Weimann, J. Phys. C **18**, L257 (1985).

[11] H.Z. Zheng, D.C. Tsui, and A.M. Chang, Phys. Rev. B **32**, 5506 (1985).

[12] T. Ando, A.B. Fowler, and F. Stern, Rev. Mod. Phys. **54**, 437 (1982).

[13] T. Englert, D.C. Tsui, A.C. Gossard, and C. Uihlein, Surf. Sc. **113**, 295 (1982).

[14] R.R. Gerhardts, and V. Gudmundsson, Phys. Rev. B **34**, 2999 (1986) and references therein.

[15] R. Woltjer, Ph. D. thesis, Rijks Universiteit Utrecht (1988).

[16] R.J. Haug, K. von Klitzing, and K. Ploog, Phys. Rev. B **35**, 5933 (1987) and R.J. Haug, R.R. Gerhardts, K. von Klitzing, and K. Ploog, Phys. Rev. Lett. **59**, 1349 (1987).

[17] B.E. Kane, D.C. Tsui, and G. Weimann, Phys. Rev. Lett. **59**, 1353 (1987).

[18] A.M. Chang, G. Timp, T.Y. Chang, J.E. Cunningham, P.M. Mankiewich, R.E. Behringer, and R.E. Howard, Sol. St. Comm. **67**, 769 (1988).

[19] P. Hendriks, J.H. Wolter, K. de Kort, R.E. Horstman, J.-P. André, and C.T. Foxon, Sem. Sc. Technol. **3**, 521 (1988).

[20] L.A. Moretti, F.A. Chambers, G.P. Devane, and F.A. Kish, IEEE J. Quantum Electr. **25**, 1018 (1989).

[21]P.F. Fontein, P. Hendriks, J. Wolter, R. Peat, D.E. Williams, and J.-P. André, J. Appl. Phys. **64**, 3085 (1988).

[22]P.F. Fontein, P. Hendriks, J. Wolter, A. Kucernac, R. Peat, and D.E. Williams, SPIE Proc. **1028**, 197 (1989).

[23]P.F. Fontein, P. Hendriks, J.H. Wolter, A. Kucernac, R. Peat, and D.E. Williams, Sem. Sc. Technol. **4**, 837 (1989).

[24]P. Hendriks, F.J.M. Schnitzeler, J.E.M. Haverkort, J.H. Wolter, Kees de Kort, and G. Weimann, Appl. Phys. Lett. **54**, 1763 (1989).

[25]A. Yariv, Quantum Electronics (Wiley, New York, 1967).

[26]B.H. Kolner, and D.M. Bloom, IEEE J. Quantum Electron. **22**, 79 (1986).

[27]A.H. MacDonald, T.M. Rice, and W.F. Brinkman, Phys. Rev. B **28**, 3648 (1983).

[28]D.J. Thouless, J. Phys. **C18**, 6211 (1985)

[29]C.W.J. Beenakker and H. van Houten, to be publ. in Solid State Physics, Academic Press, New York 1991, H. Ehrenreich and D. Turnbull eds..

[30]D.A. Syphers, K.P. Martin, and R.J. Higgins, Appl. Phys. Lett. **48**, 293 (1986).

[31]D.A. Syphers, K.P. Martin, and R.J. Higgins, Surf. Sc. **170**, 222 (1986).

CURRICULUM VITAE

2-9j.

geboren:	15 september 1961 te Geldrop.
middelbaar onderwijs:	Augustinianum Eindhoven, Gymnasium B, van augustus 1973 tot mei 1979.
universiteit:	Technische Universiteit Eindhoven, Faculteit der Technische Natuurkunde, van augustus 1979 tot september 1986.
promotie onderzoek:	Technische Universiteit Eindhoven, Faculteit der Technische Natuurkunde, groep Halfgeleiderfysica, van 15 september 1986 tot 15 september 1990, in dienst van de Stichting voor Fundamenteel Onderzoek der Materie (FOM).

LIST OF PUBLICATIONS

1 P.F. Fontein, J.M. Lagemaat, J.H. Wolter, and J.-P. André, Magnetic field modulation – a method for measuring the Hall conductance on a Corbino disc, Semicond. Sci. Technol. **3**, 915–918 (1988).

2 P.F. Fontein, P. Hendriks, J.H. Wolter, R. Peat, D.E. Williams, and J.-P. André, Use of the lateral photo effect to study sample quality in GaAs/Al$_x$Ga$_{1-x}$As heterostructures, J. Appl. Phys. **64**, 3085–3088 (1988).

3 J.H. Wolter, F.A.P. Blom, P. Koenraad, and P.F. Fontein, The influence of impurities on the Shubnikov-de Haas and Hall resistance of two-dimensional electron gases in GaAs/Al$_x$Ga$_{1-x}$As heterostructures investigated by back-gating and persistent photo-conductivity, Nato ASI Series Vol. 183, 297–305 (1989), C.Y. Fong ed..

4 P.F. Fontein, P. Hendriks, J.H. Wolter, A. Kucernak, R. Peat, and D.E. Williams, Topography of GaAs/Al$_x$Ga$_{1-x}$As heterostructures using the lateral photo effect, SPIE Proc. **1028**, Scanning Imaging, 197–201 (1989).

5 P.F. Fontein, P. Hendriks, J.H. Wolter, A. Kucernak, R. Peat, and D.E. Williams, Differential measurements of the lateral photo effect in GaAs/Al$_x$Ga$_{1-x}$As heterostructures, Semicond. Sci. Technol. **4**, 837–840 (1989).

6 idem. in Engineering Optics 53–56 (Feb. 1990).

7 F.A.P. Blom, P.F. Fontein, J.H. Wolter, F.M. Peeters, X. Wu, F. Geerinckx, and J.T. Devreese, Temperature dependence of the amplitude of the Shubnikov-de Haas oscillations in a two-dimensional electron gas, Surf. Sc. **229**, 70–72 (1990).

8   P.F. Fontein, P. Hendriks, and J.H. Wolter, Contactless measurement of the local potential distribution in the quantum Hall effect, Surf. Sc. **229**, 47–49 (1990).

9   P.F. Fontein, J.A. Kleinen, P. Hendriks, F.A.P. Blom, J.H. Wolter, H.G.M. Lochs, F.A.J.M. Driessen, and L.J. Giling, The spatial potential distribution in $GaAs/Al_xGa_{1-x}As$ heterostructures under quantum Hall conditions studied with the linear electro-optic effect, accepted for publication in Springer Series in Solid State Sciences, Springer Verlag (Berlin), K. von Klitzing ed..

10 P.F. Fontein, J.A. Kleinen, P. Hendriks, F.A.P. Blom, J.H. Wolter, H.G.M. Lochs, F.A.J.M. Driessen, L.J. Giling, and C.W.J. Beenakker, The spatial potential distribution in $GaAs/Al_xGa_{1-x}As$ heterostructures under quantum Hall conditions studied with the linear electro-optic effect, submitted to Phys. Rev. B rap. comm..

11 P.F. Fontein, J.A. Kleinen, P. Hendriks, F.A.P. Blom, J.H. Wolter, H.G.M. Lochs, F.A.J.M. Driessen, L.J. Giling, and C.W.J. Beenakker, spatially resolved potential measurements under quantum Hall conditions by application of the linear electro-optic effect, accepted for presentation at the 20th Int. Conf. on the Physics of Semiconductors, Thessaloniki, 1990, to be published.

1 Kleine inhomogeniteiten in de electronenconcentratie kunnen de stroomverdeling in hoge magneetvelden sterk beïnvloeden.
    – *Dit proefschrift, hoofdstuk 4.*

2 In quantum Hall plateaus is het Hall electrisch veld geconcentreerd aan de randen van de Hall bar structuur.
    – *Dit proefschrift, hoofdstuk 5.*

3 Ten gevolge van het verschil in geometrie tussen de Hall bar en de Corbino disk heeft een inhomogene electronenconcentratie in beide geometrieën een tegengestelde invloed op het al dan niet optreden van het quantum Hall effect.
    – *Dit proefschrift, hoofdstuk 6.*

4 Vele modellen hebben vrijwel geen voorspellende werking.
    – *Het is eenvoudiger het model aan het experiment aan te passen dan andersom.*

5 Het laterale fotoeffect is op zijn minst tweemaal herontdekt.
    – *T. Wallmark, Proc. IRE 45, 474 (1957).*
    – *P.F. Fontein, P. Hendriks, J.H. Wolter, R. Peat, D.E. Williams, and J.-P. André, J. Appl. Phys. 64, 3085 (1988).*
    – *N. Tabatabaie, M.-H. Meynadier, R.E. Nahory, J.P. Harbison, and L.T. Florez, Appl. Phys. Lett. 55, 792 (1989).*

6   De effectieve massa zoals bepaald met behulp van Ando's formule uit
     Shubnikov-de Haas metingen heeft niets te maken met de cyclotron effectieve
     massa.

     – *F.A.P. Blom, P.F. Fontein, J.H. Wolter, F.M. Peeters, X. Wu,
       F. Geerinckx, and J.T. Devreese, Surf. Sc. **229**, 70 (1990).*

7   De voortgang van de fysica kan belemmerd worden door een te groot
     enthousiasme voor een bepaald model.

     – *M. Büttiker, Phys. Rev. B **38**, 9375 (1988).*

8   De bepaling van de effectieve g-factor in $GaAs/Al_xGa_{1-x}As$ heterostructuren uit
     de temperatuurafhankelijkheid van het Shubnikov-de Haas effect berust op
     teveel vooronderstellingen om betrouwbaar te zijn.

     – *T. Englert, D.C. Tsui, A.C. Gossard, and C. Uihlein, Surf. Sc. **113**, 295
       (1982).*

9   Lieveheersbeestjes vliegen meestal weg als ze het topje van een opgestoken
     vinger bereikt hebben.

     – *Eigen waarneming, vier uit zes gevallen.*

Eindhoven, 5 oktober 1990   Peter Fontein